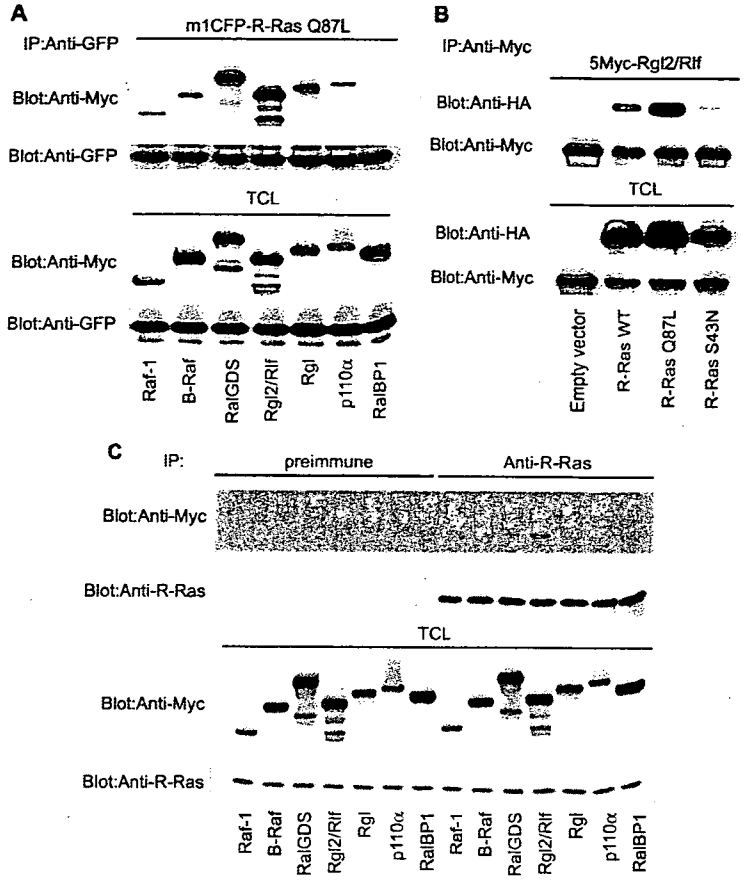

Figure 4. Binding of R-Ras to Rgl2/Rlf. (A) Cos7 cells expressing mCFP-tagged R-Ras-Q87L and the Myc-tagged effector proteins indicated at the bottom of the panel were used for the analysis. In p110α expression, p85α was used for coexpression to stabilize the PI3K heterodimer complex. From the cell lysates, GFP-tagged proteins were immunoprecipitated, and bound proteins were analyzed by immunoblotting with anti-Myc mAb or anti-GFP mAb. (B) Cos7 cells expressing HA-tagged R-Ras mutants and Myc-tagged Rgl2/Rlf were lysed and analyzed as described in A. (C) Endogenous R-Ras protein was immunoprecipitated with anti-R-Ras serum from Cos7 cells expressing the Myc-tagged effector proteins. The immunoprecipitates were analyzed as described in A. Preimmune serum was used as a control.

spinning disk confocal unit (Figure 3C). To exclude the possibility that the high FRET level on the endosomes was caused by accumulation of the probe, we used control probes, i.e., Raichu-R-Ras G38V and Raichu-R-Ras S43N, the properties of which are shown in Supplemental Figure S3. The FRET level was diffusely high on both the plasma membrane and on endosomes in cells expressing Raichu-R-Ras G38V (Figure 3, C and D). In contrast, cells expressing Raichu-R-Ras S43N showed low levels of FRET, both on the plasma membrane and on endosomes (Figure 3, C and D). The intensity of the probe on each endosome did not affect the emission ratio of sensitized FRET over CFP in either the Raichu-R-Ras wild type, G38V mutant, or S43N mutant (data not shown). Therefore, these results negated the possibility that the high FRET signal observed on the endosomes of Raichu-R-Ras–expressing cells was caused by an accumulation of the probe. Interestingly, we could not observe remarkable difference in the localization of the wild-type and mutant Raichu-Ras proteins. This is probably because the effector domain of R-Ras-GTP is masked by the Ras-binding domain of the probe and suggests that the localization of the probe was determined primarily by the carboxy terminus of R-Ras.

Endosomal Localization of Rgl2/Rlf, an R-Ras Effector

Next, we attempted to identify the signaling molecules downstream of R-Ras on the endosomes. To this end, we first compared the affinity of R-Ras for Raf-1, B-Raf, RalGDS, Rgl2/Rlf, Rgl, and the p110α subunit of PI3K, all of which are known to bind to a wide range of Ras-family GTPases (Figure 4A). K-Ras and Rap1A were used as controls for the GTPases (Supplemental Figure S5A). In a coimmunoprecipitation assay, a constitutively active mutant of R-Ras (R-Ras Q87L) was found to interact most strongly with three GEFs for Ral, i.e., RalGDS, Rgl, and Rgl2/Rlf, and less strongly with Raf-1, B-Raf, and p110α. These interactions were shown to depend on GTP loading, because the R-Ras Q87L mutant showed a markedly higher affinity for Rgl2/Rlf than did the wild-type protein and the nucleotide-free mutant, R-Ras S43N (Figure 4B). However, it should be noted that the high-affinity binding detected by coimmunoprecipitation does not necessarily indicate the signaling strength between the two associated proteins. Thus, we examined the effect of the activated R-Ras mutant, R-Ras Q87L, on the activity of downstream effectors. In agreement with the coimmunoprecipitation experiments, RalA, RalB, and Akt1 (downstream of p110 PI3K), but not MEK1 (downstream of the Raf proteins), were activated by R-Ras Q87L (Supplemental Figure S5). Next, we used R-Ras antiserum to examine whether the endogenous R-Ras protein is also associated with Ras effectors. Among the effector proteins tested, Rgl2/Rlf exhibited the strongest affinity for endogenous R-Ras (Figure 4C). Finally, we confirmed that Rgl2/Rlf, but not Raf-1 or p110α, colocalized efficiently with R-Ras on the endosomes (Figure 5, A and B). This endosomal colocalization of Rgl2/Rlf with R-Ras was abrogated by the expression of R-RasGAP (Figure 5C). These results strongly suggested that R-Ras is bound to Rgl2/Rlf on endosomes in a GTP-dependent manner.

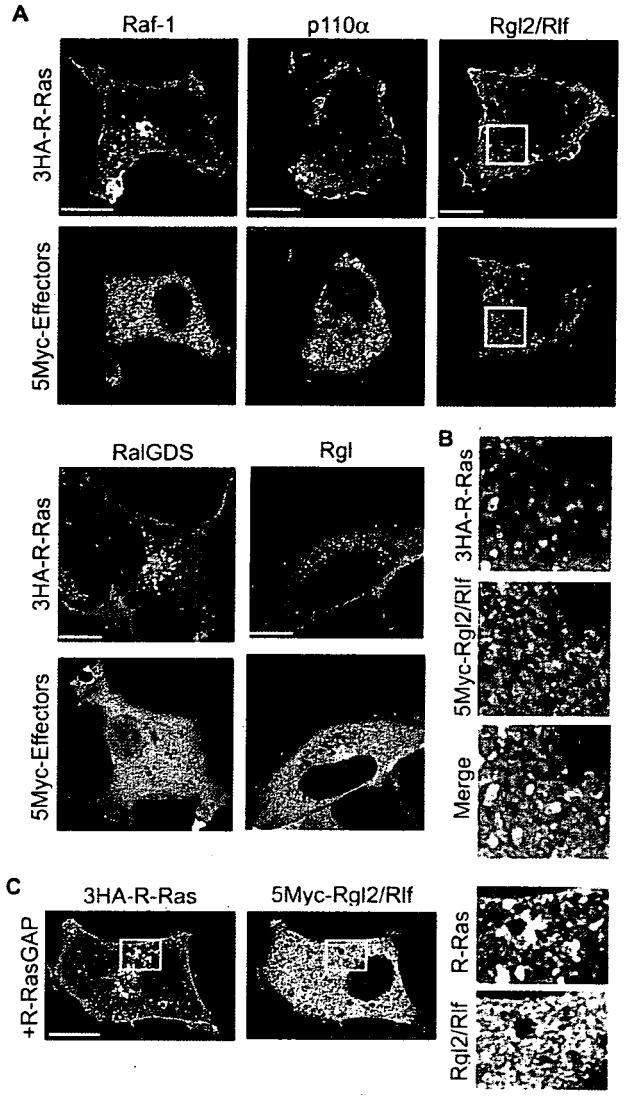

Figure 5. Colocalization of R-Ras with Rgl2/Rlf. (A) Cos7 cells expressing HA-tagged R-Ras and Myc-tagged R-Ras effector proteins were stained with anti-HA and anti-Myc antibodies, and the cells were observed by confocal microscopy. Bar, 10 μm. (B) Enlarged images of the outlined regions in A. In the merged image, green and red indicate 3HA-R-Ras and 5Myc-Rgl2/Rlf, respectively. (C) Cos7 cells expressing HA-tagged R-Ras, Myc-tagged Rgl2/Rlf, and R-RasGAP were stained with anti-HA and anti-Myc antibodies. Right panels are enlarged images of the outlined regions in the left panels.

Regulation of Vesicular RalA Activity by R-Ras

We next addressed the question of whether R-Ras regulates the activities of Ral proteins on the endosomes. In results that were consistent with those of a previous report (Shipitsin and Feig, 2004), RalA and RalB were detected both on the plasma membrane and on endosomes (Supplemental Figure S4C). Because colocalization with R-Ras was clearer in the case of RalA than RalB, we focused on RalA and examined the RalA activity on endosomes by use of Raichu-RalA, a marker for RalA activity (Takaya *et al.*, 2004) (Figure 6). In contrast to the FRET images obtained with Raichu-R-Ras, the FRET level varied significantly among endosomes, suggesting that RalA activity varied among different types of endosomes (Figure 6A). We considered it likely that such differences in RalA activity among endosomes might have depended on the presence of active R-Ras; therefore, we examined RalA activity in cells expressing R-RasGAP or shRNA for R-Ras. Under both conditions, the number of endosomes showing high RalA activity was reduced significantly (Figure 6, B–D). This shRNA-mediated decrease in RalA activity was recovered by the coexpression of exogenous R-Ras, the cDNA of which harbors mutations in the shRNA-binding sequence. The dependence of RalA activity on R-Ras was confirmed by a pull-down assay with the RalA-binding region of RalBP1; the net amount of GTP-RalA was thus shown to have decreased by 20% (Figure 6E). It should be noted that the basal GTP level of RalA is ~7% of total guanine nucleotides bound to RalA (Takaya *et al.*, 2004). Therefore, if we assume based on the immunofluorescence data that the proportion of RalA on the endosomes is significantly smaller than that at the plasma membrane, a 20% decrease in the net amount of GTP-RalA seemed to be consistent with the significant reduction in the number of endosomes showing a high GTP-RalA level, as demonstrated by Raichu-RalA. Finally, we found that knockdown of Rgl2/Rlf profoundly decreased the RalA activity on the endosomes, suggesting that the R-Ras–Rgl2/Rlf complex is the principal activator of RalA on the endosomes (Figure 6F).

Requirement of R-Ras and RalA for Calcium-dependent Exocytosis

It has been reported that RalA is engaged in calcium-triggered exocytosis (Moskalenko *et al.*, 2002; Vitale *et al.*, 2005), which prompted us to examine the role played by R-Ras in the same process. YFP-tagged NPY and rat growth hormone (rGH) were used as markers of exocytosis (Nagai *et al.*, 2002; Matsuno *et al.*, 2005) (Figure 7 and Supplemental Figure S4C). In PC12 cells, depolarization-induced NPY secretion was as significantly inhibited by the expression of active R-Ras (Q87L) and R-RasGAP as by the expression of active RalA (G23V) and Rab11a (Q70L). The expression levels of recombinant proteins were examined by a quantitative immunoblotting analysis (Supplemental Figure S6). Because the expression of Rab11a T22N was less than R-Ras or RalA mutants, the ineffectiveness of this particular mutant might be ascribable to its low expression level. The role played by R-Ras and RalA was further confirmed with small interfering RNA (siRNA) (Figure 7B). The reduction of R-Ras and RalA inhibited depolarization-induced NPY secretion to a similar extent. Among the three Ral GEFs knocked down by siRNA, only the reduction of Rgl2/Rlf had an inhibitory effect on NPY secretion (Figure 7C). In GH3 pituitary adenoma cells, in which the level of expression of endogenous R-Ras was found to be low, the exogenous expression of R-Ras significantly enhanced the depolarization-induced exocytosis of both rGH and NPY (Figure 7D). The enhancement by R-Ras was abrogated by the knockdown of either R-Ras or RalA (Figure 7E). These results demonstrated that R-Ras is involved in depolarization-induced exocytosis, most likely due to the activation of Ral proteins. Furthermore, the finding that not only inhibition but also constitutive activation of R-Ras inhibits exocytosis suggests that the on-off cycle of R-Ras is required for this process.

DISCUSSION

We propose the following scenario for the role of R-Ras on endosomes: 1) R-Ras is activated on the surface of recycling and early endosomes, and it remains active on the vesicles

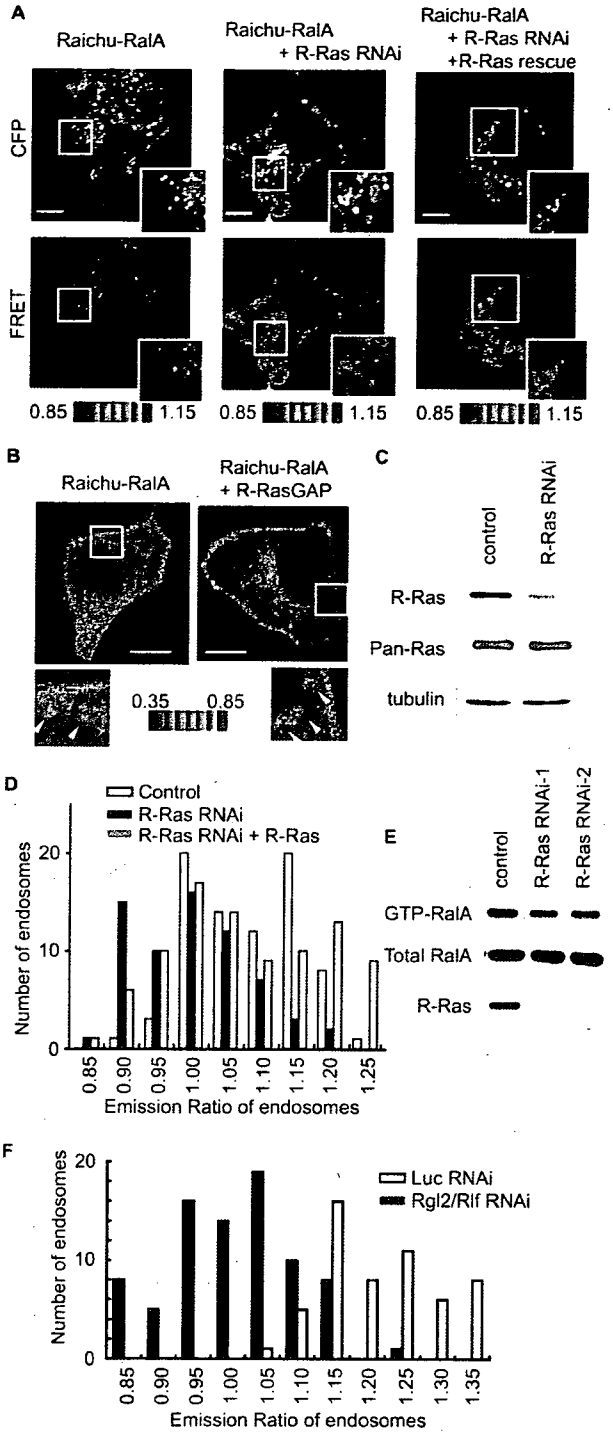

Figure 6. Effect of R-Ras knockdown on RalA activity on the endosomes. (A) Cos7 cells were transfected with expression vectors as indicated at the top of the panel. For knockdown, we used pSuper-R-Ras, an shRNA vector. For the rescue from knockdown, an R-Ras mutant resistant to the shRNA vector was expressed. Sixty hours after transfection, CFP and FRET images were obtained with a spinning confocal microscope. (B) MDCK cells were transfected with expression vectors as indicated at the top of the panel and imaged 20 h after transfection as in A. Outlined regions were enlarged and are shown in the insets. Arrowheads indicate representative vesicles. Bar, 10 μm. (C) Cells transfected with an empty pSuper vector and pSuper-R-Ras were selected as described in A, and the proteins were analyzed by immunoblotting with the antibodies shown on the left. (D) Histogram of the FRET level of Raichu-RalA on the endosomes. The histograms were drawn from the data obtained from 79 endosomes in four Cos7 cells, those obtained from 66 endosomes in six pSuper-R-Ras–expressing Cos7 cells and those obtained from 89 endosomes in nine Cos7 cells expressing both pSuper-R-Ras and pCXN2-5Myc-R-Ras-rRNAi. (E) HeLa cells were transfected with control siRNA or two different siRNAs for R-Ras. After 72 h, GTP-RalA levels in the cells were analyzed by Bos' pull-down method with GST-RalBP1-RBD. The knockdown of R-Ras was also confirmed by immunoblotting. (F) The histograms were drawn from the data obtained from 55 endosomes in two Raichu-RalA-expressing Cos7 cells transfected with siRNA for luciferase and those obtained from 83 endosomes in three Raichu-RalA–expressing Cos7 cells transfected with siRNA for Rgl2/Rlf.

derived from these endosomes. 2) The active R-Ras on these vesicles recruits Ral GEF(s). Among the candidate proteins, Rgl2/Rlf is the most plausible, because R-Ras activates both Rgl and Rgl2/Rlf more efficiently than it does RalGDS (Rodriguez-Viciana *et al.*, 2004), and also because the endogenous R-Ras was found to colocalize with Rgl2/Rlf (Figure 5). However, other Ral GEFs that are also known to bind to R-Ras (Nancy *et al.*, 1999; Shao and Andres, 2000; Rodriguez-Viciana *et al.*, 2004) may be recruited to R-Ras on endosomes in other cell types. 3) These R-Ras-recruited Ral GEFs on the endosomes activate RalA, followed by the recruitment of RalA effectors to the endosomes. Among these effectors is Exo84, a component of the exocyst complex, which marks a microdomain at the plasma membrane as a delivery site for exocytotic vesicles (Grindstaff *et al.*, 1998; Yeaman *et al.*, 2001; Inoue *et al.*, 2003). 4) The R-Ras-loaded vesicles from endosomes are tethered to the plasma membrane via the exocyst complex. It has been demonstrated that the interaction between RalA and the exocyst complex is essential for exocytosis (Moskalenko *et al.*, 2002; Polzin *et al.*, 2002; Shipitsin and Feig, 2004), and the inhibition of the exocyst complex has been shown to impair calcium-triggered exocytosis (Tsuboi *et al.*, 2005). Therefore, our observations that R-Ras was required for the calcium-induced secretion of NPY and rGH (Figure 7) are suggestive of the positive role played by R-Ras in the formation of the exocyst complex.

Another prediction contained in our model, but not directly assessed, is that RalA regulates the assembly of the exocyst complex, both on the vesicles and on the plasma membrane, by means of binding to different components of the exocyst complex: RalA interacts not only with Exo84 but also with Sec5, another component of the exocyst complex (Feig, 2003). Sec5 is primarily present on the plasma membrane, whereas Exo84 is localized primarily on the vesicles (Moskalenko *et al.*, 2003). In this context, it should be noted that RalA is activated on the plasma membrane either by Ras-dependent or by calcium-dependent pathways (Hofer *et al.*, 1998; Wolthuis and Bos, 1999). Hence, the tethering of vesicles may be promoted by the two portions of the exocyst complex, both of which are anchored to the lipid membranes via RalA. One portion consists of subunits containing Exo84 and is anchored to the endosomes and/or the vesicles and endosomes by R-Ras-activated RalA, whereas the other portion consists of subunits containing Sec5, and it is anchored to the plasma membrane by RalA activated by either Ras or calcium. The results have thus far suggested that the high activity of R-Ras and RalA on the surface of vesicles is constitutive rather than stimulation regulated. Therefore, RalA activity at the plasma membrane, but not that on

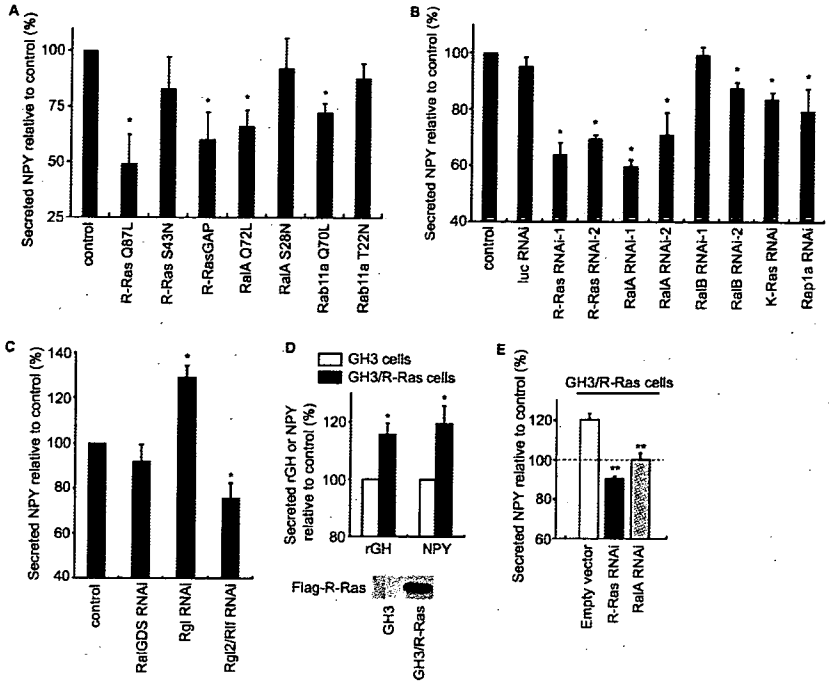

Figure 7. Requirement of both R-Ras and RalA for depolarization-induced exocytosis. (A) PC12 cells were transfected with pVenus-NPY together with the indicated constructs. Sixty hours after transfection, the cells were stimulated with high-potassium saline for 20 min. The efficiency of NPY-Venus secretion was determined as the ratio of NPY-Venus present in the medium versus that remaining in the cell lysates. The values were normalized to a vector control. Error bars indicate the SD from at least three experiments. The symbols indicate the results of *t* test analysis; *$p < 0.002$ compared with the control. (B and C) PC12 cells were transfected with pVenus-NPY and siRNA for luciferase, R-Ras, RalA, RalB, RalGDS, Rgl, or Rgl2/Rlf. NPY secretion upon depolarization was examined as described in A. Error bars indicate the SD from at least three experiments. The symbols indicate the results of *t* test analysis; *$p < 0.001$ compared with the control. (D) GH3 cells and GH3/R-Ras cells were transfected with expression vectors for NPY-Venus or EYFP-GH1. Depolarization-induced secretion was monitored as described in A. The symbols indicate the results of *t* test analysis; *$p < 0.001$ compared with the control. (E) GH3/R-Ras cells were transfected with expression vectors for NPY-Venus and an shRNA vector for R-Ras, or RalA. Depolarization-induced secretion of NPY was examined as described in A. The symbols indicate the results of *t* test analysis; **$p < 0.001$ compared with the control (GH3/R-Ras cells).

endosomes, may play a regulatory role in the assembly of the complete exocyst complex. In agreement with this view, we have shown that RalA is locally activated in the nascent lamellipodia of epidermal growth factor (EGF)-stimulated or migrating cells (Takaya *et al.*, 2004). Because exocytosis plays critical roles in EGF-induced membrane ruffling and cell migration (Bretscher and Aguado-Velasco, 1998; Schmoranzer *et al.*, 2003; Proux-Gillardeaux *et al.*, 2005; Tayeb *et al.*, 2005), RalA activation at the site of the membrane protrusion may indicate its role in the transport of lipid bilayer and/or integral proteins via exocytosis.

In agreement with the results of a previous report showing that RalA but not RalB regulates the delivery of E-cadherin in MDCK cells (Shipitsin and Feig, 2004), we found that only RalA was involved in calcium-triggered exocytosis (Figure 7). This difference between the two Ral proteins with respect to their involvement in exocytosis may be ascribable not only to the low binding affinity of RalB to Sec5 (Shipitsin and Feig, 2004) but also to the predominant localization of RalB on the plasma membrane (Shipitsin and Feig, 2004; Lim *et al.*, 2005).

Currently, the mechanism underlying the high R-Ras activity on the endosomes remains unknown. A dominant-negative mutant of R-Ras has been shown to be more enriched on endosomes than is the wild-type protein (Furuhjelm and Peranen, 2003). Because a dominant-negative mutant of Ras family GTPases sequesters GEFs (Feig, 1999), these observations strongly suggest that the GEFs for R-Ras are enriched on endosomes. In contrast to RalA on the vesicles, the activity of R-Ras on the vesicles seems constant (Figures 3C and 6A). Thus, R-Ras may be activated as soon as nascent R-Ras is recruited to the vesicles and inactivated when the vesicles are fused to the plasma membrane. Although none of the GEFs for R-Ras (i.e., RasGRF1, CalDAG-GEF-I/RasGRP2, CalDAG-GEF-II/RasGRP1, CalDAG-GEF-III/RasGRP3, and C3G) have been shown to localize on the endosomes (Ohba *et al.*, 2000), this failure to detect GEFs on the endosomes may simply reflect a lack of high-affinity antibodies that could be applied for immunostaining. Interestingly, GAPs for R-Ras seem to localize primarily on the plasma membrane (Anderson *et al.*, 1990; Margolis *et al.*, 1990; Cozier *et al.*, 2003; Oinuma *et al.*, 2004). Thus, R-Ras would be expected to be inactivated when it is transported from the endosomes to the plasma membrane. This inactivation of R-Ras might serve to liberate the components of the exocyst complex and send them back into the cytoplasm or to send R-Ras back to the endosomes from the plasma membrane.

Previous studies have implicated R-Ras in the activation of integrin (Zhang *et al.*, 1996; Keely *et al.*, 1999; Berrier *et al.*, 2000; Self *et al.*, 2001; Oinuma *et al.*, 2006) and also in cell migration and adhesion (Nakada *et al.*, 2005; Wozniak *et al.*, 2005); however, the molecular mechanisms underlying these phenomena remain elusive. Our finding that the R-Ras-Rgl2/Rlf-RalA pathway regulates exocytosis may account for some of these biological activities of R-Ras. It is already known that the inhibition of exocytosis impairs integrin recycling and thereby also cell migration and cell adhesion (Proux-Gillardeaux *et al.*, 2005; Tayeb *et al.*, 2005). Hence, the inhibition of integrin by the suppression of R-Ras might initially be caused by the disruption of exocytosis. Although no direct evidence supporting the involvement of RalA in the recycling of integrin has yet been reported, Ral proteins have been shown to be implicated in cell migration (Gildea *et al.*, 2002; Takaya *et al.*, 2004; Oxford *et al.*, 2005), a process in which integrin is thought to be coordinately activated and inactivated. Therefore, it is reasonable to speculate that the R-Ras-Rgl2/Rlf-RalA pathway is involved in the recycling of integrin and thereby also in the regulation of integrin activity.

In conclusion, we observed high R-Ras activity on early and recycling endosomes. This high R-Ras activity recruits Rlf/Rgl2 and thereby activates RalA, followed by the assembly of a portion of the exocyst complex. Importantly, in

addition to RalA, other low-molecular-weight GTPases belonging to different families (i.e., TC10, Arf6, and Rab11) are also known to interact with the exocyst complex (Prigent *et al.*, 2003; Inoue *et al.*, 2003; Zhang *et al.*, 2004; Wu *et al.*, 2005). Further study will be needed to determine whether these GTPases of different families coordinately regulate the exocyst complex on the same endosomes, or whether there are distinct classes of endosomes containing only some of these GTPases. It would be of particular importance to examine the dynamic activity changes of these GTPases during the vesicular transport, which would be best examined by FRET-based imaging techniques used here.

ACKNOWLEDGMENTS

We thank L. A. Feig, R. Y. Tsien, Y. Fukui, K. Kaibuchi, A. Kikuchi, S. Kuroda, B. J. Mayer, N. Minato, A. Miyawaki, and Y. Takai for the provision of reagents and N. Yoshida, N. Fujimoto, and K. Fukuhara for technical assistance. This work was supported by grants-in-aid for scientific research and for cancer research from the Ministry of Education, Science, Sports and Culture of Japan, and by a grant from the Health Science Foundation of Japan. A.T. was supported by Research Fellowships from the Japan Society for the Promotion of Science for Young Scientists.

REFERENCES

Akagi, T., Sasai, K., and Hanafusa, H. (2003). Refractory nature of normal human diploid fibroblasts with respect to oncogene-mediated transformation. Proc. Natl. Acad. Sci. USA *100*, 13567–13572.

Anderson, D., Koch, C. A., Grey, L., Ellis, C., Moran, M. F., and Pawson, T. (1990). Binding of SH2 domains of phospholipase C gamma 1, GAP, and Src to activated growth factor receptors. Science *250*, 979–982.

Aoki, K., Nakamura, T., Fujikawa, K., and Matsuda, M. (2005). Local phosphatidylinositol 3,4,5-trisphosphate accumulation recruits Vav2 and Vav3 to activate Rac1/Cdc42 and initiate neurite outgrowth in nerve growth factor-stimulated PC12 cells. Mol. Biol. Cell *16*, 2207–2217.

Berrier, A. L., Mastrangelo, A. M., Downward, J., Ginsberg, M., and LaFlamme, S. E. (2000). Activated R-ras, Rac1, PI 3-kinase and PKCepsilon can each restore cell spreading inhibited by isolated integrin beta1 cytoplasmic domains. J. Cell Biol. *151*, 1549–1560.

Bretscher, M. S., and Aguado-Velasco, C. (1998). EGF induces recycling membrane to form ruffles. Curr. Biol. *8*, 721–724.

Cox, A. D., Brtva, T. R., Lowe, D. G., and Der, C. J. (1994). R-Ras induces malignant, but not morphologic, transformation of NIH3T3 cells. Oncogene *9*, 3281–3288.

Cozier, G. E., Bouyoucef, D., and Cullen, P. J. (2003). Engineering the phosphoinositide-binding profile of a class I pleckstrin homology domain. J. Biol. Chem. *278*, 39489–39496.

Feig, L. A. (1999). Tools of the trade: use of dominant-inhibitory mutants of Ras-family GTPases. Nat. Cell Biol. *1*, E25–E27.

Feig, L. A. (2003). Ral-GTPases: approaching their 15 minutes of fame. Trends Cell Biol. *13*, 419–425.

Finger, F. P., Hughes, T. E., and Novick, P. (1998). Sec3p is a spatial landmark for polarized secretion in budding yeast. Cell *92*, 559–571.

Friedrich, G. A., Hildebrand, J. D., and Soriano, P. (1997). The secretory protein Sec8 is required for paraxial mesoderm formation in the mouse. Dev. Biol. *192*, 364–374.

Furuhjelm, J., and Peranen, J. (2003). The C-terminal end of R-Ras contains a focal adhesion targeting signal. J. Cell Sci. *116*, 3729–3738.

Gildea, J. J., Harding, M. A., Seraj, M. J., Gulding, K. M., and Theodorescu, D. (2002). The role of Ral A in epidermal growth factor receptor-regulated cell motility. Cancer Res. *62*, 982–985.

Gonzalez-Garcia, A., Pritchard, C. A., Paterson, H. F., Mavria, G., Stamp, G., and Marshall, C. J. (2005). RalGDS is required for tumor formation in a model of skin carcinogenesis. Cancer Cell *7*, 219–226.

Gotoh, T., Niino, Y., Tokuda, M., Hatase, O., Nakamura, S., Matsuda, M., and Hattori, S. (1997). Activation of R-Ras by Ras-guanine nucleotide-releasing factor. J. Biol. Chem. *272*, 18602–18607.

Grindstaff, K. K., Yeaman, C., Anandasabapathy, N., Hsu, S. C., Rodriguez-Boulan, E., Scheller, R. H., and Nelson, W. J. (1998). Sec6/8 complex is recruited to cell-cell contacts and specifies transport vesicle delivery to the basal-lateral membrane in epithelial cells. Cell *93*, 731–740.

Gromley, A., Yeaman, C., Rosa, J., Redick, S., Chen, C. T., Mirabelle, S., Guha, M., Sillibourne, J., and Doxsey, S. J. (2005). Centriolin anchoring of exocyst and SNARE complexes at the midbody is required for secretory-vesicle-mediated abscission. Cell *123*, 75–87.

Hamad, N. M., Elconin, J. H., Karnoub, A. E., Bai, W., Rich, J. N., Abraham, R. T., Der, C. J., and Counter, C. M. (2002). Distinct requirements for Ras oncogenesis in human versus mouse cells. Genes Dev. *16*, 2045–2057.

Hofer, F., Berdeaux, R., and Martin, G. S. (1998). Ras-independent activation of Ral by a Ca(2+)-dependent pathway. Curr. Biol. *8*, 839–842.

Huff, S. Y., Quilliam, L. A., Cox, A. D., and Der, C. J. (1997). R-Ras is regulated by activators and effectors distinct from those that control Ras function. Oncogene *14*, 133–143.

Inoue, M., Chang, L., Hwang, J., Chiang, S. H., and Saltiel, A. R. (2003). The exocyst complex is required for targeting of Glut4 to the plasma membrane by insulin. Nature *422*, 629–633.

Keely, P. J., Rusyn, E. V., Cox, A. D., and Parise, L. V. (1999). R-Ras signals through specific integrin alpha cytoplasmic domains to promote migration and invasion of breast epithelial cells. J. Cell Biol. *145*, 1077–1088.

Komatsu, M., and Ruoslahti, E. (2005). R-Ras is a global regulator of vascular regeneration that suppresses intimal hyperplasia and tumor angiogenesis. Nat. Med. *11*, 1346–1350.

Kurokawa, K., Itoh, R. E., Yoshizaki, H., Nakamura, T., and Matsuda, M. (2004a). Coactivation of Rac1 and Cdc42 at lamellipodia and membrane ruffles induced by epidermal growth factor. Mol. Biol. Cell *15*, 1003–1010.

Kurokawa, K., Takaya, A., Terai, K., Fujioka, A., and Matsuda, M. (2004b). Visulalizing the signal transduction pathways in living cells with GFP-based FRET probes. Acta Histochem. Cytochem. *37*, 347–355.

Lim, K. H., Baines, A. T., Fiordalisi, J. J., Shipitsin, M., Feig, L. A., Cox, A. D., Der, C. J., and Counter, C. M. (2005). Activation of RalA is critical for Ras-induced tumorigenesis of human cells. Cancer Cell *7*, 533–545.

Lipschutz, J. H., and Mostov, K. E. (2002). Exocytosis: the many masters of the exocyst. Curr. Biol. *12*, R212–R214.

Lowe, D. G., Capon, D. J., Delwart, E., Sakaguchi, A. Y., Naylor, S. L., and Goeddel, D. V. (1987). Structure of the human and murine R-ras genes, novel genes closely related to ras proto-oncogenes. Cell *48*, 137–146.

Margolis, B., Li, N., Koch, A., Mohammadi, M., Hurwitz, D. R., Zilberstein, A., Ullrich, A., Pawson, T., and Schlessinger, J. (1990). The tyrosine phosphorylated carboxy terminus of the EGF receptor is a binding site for GAP and PLC-gamma. EMBO J. *9*, 4375–4380.

Marte, B. M., Rodriguez-Viciana, P., Wennstrom, S., Warne, P. H., and Downward, J. (1997). R-Ras can activate the phosphoinositide 3-kinase but not the MAP kinase arm of the Ras effector pathways. Curr. Biol. *7*, 63–70.

Matsuno, A., Mizutani, A., Itoh, J., Takekoshi, S., Nagashima, T., Okinaga, H., Takano, K., and Osamura, R. Y. (2005). Establishment of stable GH3 cell line expressing enhanced yellow fluorescein protein-growth hormone fusion protein. J. Histochem. Cytochem. *53*, 1177–1180.

Mochizuki, N., Yamashita, S., Kurokawa, K., Ohba, Y., Nagai, T., Miyawaki, A., and Matsuda, M. (2001). Spatio-temporal images of growth-factor-induced activation of Ras and Rap1. Nature *411*, 1065–1068.

Moskalenko, S., Henry, D. O., Rosse, C., Mirey, G., Camonis, J. H., and White, M. A. (2002). The exocyst is a Ral effector complex. Nat. Cell Biol. *4*, 66–72.

Moskalenko, S., Tong, C., Rosse, C., Mirey, G., Formstecher, E., Daviet, L., Camonis, J., and White, M. A. (2003). Ral GTPases regulate exocyst assembly through dual subunit interactions. J. Biol. Chem. *278*, 51743–51748.

Murthy, M., Garza, D., Scheller, R. H., and Schwarz, T. L. (2003). Mutations in the exocyst component Sec5 disrupt neuronal membrane traffic, but neurotransmitter release persists. Neuron *37*, 433–447.

Nagai, T., Ibata, K., Park, E. S., Kubota, M., Mikoshiba, K., and Miyawaki, A. (2002). A variant of yellow fluorescent protein with fast and efficient maturation for cell-biological applications. Nat. Biotechnol. *20*, 87–90.

Nakada, M., Niska, J. A., Tran, N. L., McDonough, W. S., and Berens, M. E. (2005). EphB2/R-Ras signaling regulates glioma cell adhesion, growth, and invasion. Am. J. Pathol. *167*, 565–576.

Nakashima, S., Morinaka, K., Koyama, S., Ikeda, M., Kishida, M., Okawa, K., Iwamatsu, A., Kishida, S., and Kikuchi, A. (1999). Small G protein Ral and its downstream molecules regulate endocytosis of EGF and insulin receptors. EMBO J. *18*, 3629–3642.

Nancy, V., Wolthuis, R. M., de Tand, M. F., Janoueix-Lerosey, I., Bos, J. L., and de Gunzburg, J. (1999). Identification and characterization of potential effector molecules of the Ras-related GTPase Rap2. J. Biol. Chem. *274*, 8737–8745.

Nishigaki, M., Aoyagi, K., Danjoh, I., Fukaya, M., Yanagihara, K., Sakamoto, H., Yoshida, T., and Sasaki, H. (2005). Discovery of aberrant expression of R-RAS by cancer-linked DNA hypomethylation in gastric cancer using microarrays. Cancer Res. *65*, 2115–2124.

Ohba, Y., Mochizuki, N., Yamashita, S., Chan, A. M., Schrader, J. W., Hattori, S., Nagashima, K., and Matsuda, M. (2000). Regulatory proteins of R-Ras, TC21/R-Ras2, and M-Ras/R-Ras3. J. Biol. Chem. *275*, 20020–20026.

Oinuma, I., Ishikawa, Y., Katoh, H., and Negishi, M. (2004). The Semaphorin 4D receptor Plexin-B1 is a GTPase activating protein for R-Ras. Science *305*, 862–865.

Oinuma, I., Katoh, H., and Negishi, M. (2006). Semaphorin 4D/Plexin-B1-mediated R-Ras GAP activity inhibits cell migration by regulating beta(1) integrin activity(2). J. Cell Biol. *173*, 601–613.

Oxford, G., Owens, C. R., Titus, B. J., Foreman, T. L., Herlevsen, M. C., Smith, S. C., and Theodorescu, D. (2005). RalA and RalB: antagonistic relatives in cancer cell migration. Cancer Res. *65*, 7111–7120.

Polzin, A., Shipitsin, M., Goi, T., Feig, L. A., and Turner, T. J. (2002). Ral-GTPase influences the regulation of the readily releasable pool of synaptic vesicles. Mol. Cell. Biol. *22*, 1714–1722.

Prigent, M., Dubois, T., Raposo, G., Derrien, V., Tenza, D., Rosse, C., Camonis, J., and Chavrier, P. (2003). ARF6 controls post-endocytic recycling through its downstream exocyst complex effector. J. Cell Biol. *163*, 1111–1121.

Proux-Gillardeaux, V., Gavard, J., Irinopoulou, T., Mege, R. M., and Galli, T. (2005). Tetanus neurotoxin-mediated cleavage of cellubrevin impairs epithelial cell migration and integrin-dependent cell adhesion. Proc. Natl. Acad. Sci. USA *102*, 6362–6367.

Quilliam, L.A., Rebhun, J. F., and Castro, A. F. (2002). A growing family of guanine nucleotide exchange factors is responsible for activation of Ras-family GTPases. Prog. Nucleic Acid Res. Mol. Biol. *71*, 391–444.

Rangarajan, A., Hong, S. J., Gifford, A., and Weinberg, R. A. (2004). Species- and cell type-specific requirements for cellular transformation. Cancer Cell *6*, 171–183.

Rey, I., Taylor-Harris, P., van Erp, H., and Hall, A. (1994). R-ras interacts with rasGAP, neurofibromin and c-raf but does not regulate cell growth or differentiation. Oncogene *9*, 685–692.

Rodriguez-Viciana, P., Sabatier, C., and McCormick, F. (2004). Signaling specificity by Ras family GTPases is determined by the full spectrum of effectors they regulate. Mol. Cell. Biol. *24*, 4943–4954.

Schmoranzer, J., Kreitzer, G., and Simon, S. M. (2003). Migrating fibroblasts perform polarized, microtubule-dependent exocytosis towards the leading edge. J. Cell Sci. *116*, 4513–4519.

Self, A. J., Caron, E., Paterson, H. F., and Hall, A. (2001). Analysis of R-Ras signalling pathways. J. Cell Sci. *114*, 1357–1366.

Shao, H., and Andres, D. A. (2000). A novel RalGEF-like protein, RGL3, as a candidate effector for rit and Ras. J. Biol. Chem. *275*, 26914–26924.

Shipitsin, M., and Feig, L. A. (2004). RalA but not RalB enhances polarized delivery of membrane proteins to the basolateral surface of epithelial cells. Mol. Cell. Biol. *24*, 5746–5756.

Spaargaren, M., and Bischoff, J. R. (1994). Identification of the guanine nucleotide dissociation stimulator for Ral as a putative effector molecule of R-ras, H-ras, K-ras, and Rap. Proc. Natl. Acad. Sci. USA *91*, 12609–12613.

Spaargaren, M., Martin, G. A., McCormick, F., Fernandez-Sarabia, M. J., and Bischoff, J. R. (1994). The Ras-related protein R-ras interacts directly with Raf-1 in a GTP-dependent manner. Biochem. J. *300*, 303–307.

Takaya, A., Ohba, Y., Kurokawa, K., and Matsuda, M. (2004). RalA activation at nascent lamellipodia of epidermal growth factor-stimulated Cos7 cells and migrating Madin-Darby canine kidney cells. Mol. Biol. Cell *15*, 2549–2557.

Tayeb, M. A., Skalski, M., Cha, M. C., Kean, M. J., Scaife, M., and Coppolino, M. G. (2005). Inhibition of SNARE-mediated membrane traffic impairs cell migration. Exp. Cell Res. *305*, 63–73.

Tsuboi, T., Ravier, M. A., Xie, H., Ewart, M. A., Gould, G. W., Baldwin, S. A., and Rutter, G. A. (2005). Mammalian exocyst complex is required for the docking step of insulin vesicle exocytosis. J. Biol. Chem. *280*, 25565–25570.

Vega, I. E., and Hsu, S. C. (2001). The exocyst complex associates with microtubules to mediate vesicle targeting and neurite outgrowth. J. Neurosci. *21*, 3839–3848.

Vitale, N., Mawet, J., Camonis, J., Regazzi, R., Bader, M. F., and Chasserot-Golaz, S. (2005). The Small GTPase RalA controls exocytosis of large dense core secretory granules by interacting with ARF6-dependent phospholipase D1. J. Biol. Chem. *280*, 29921–29928.

Wolthuis, R. M., and Bos, J. L. (1999). Ras caught in another affair: the exchange factors for Ral. Curr. Opin. Genet. Dev. *9*, 112–117.

Wozniak, M. A., Kwong, L., Chodniewicz, D., Klemke, R. L., and Keely, P. J. (2005). R-Ras controls membrane protrusion and cell migration through the spatial regulation of Rac and Rho. Mol. Biol. Cell *16*, 84–96.

Wu, S., Mehta, S. Q., Pichaud, F., Bellen, H. J., and Quiocho, F. A. (2005). Sec15 interacts with Rab11 via a novel domain and affects Rab11 localization in vivo. Nat. Struct. Mol. Biol. *12*, 879–885.

Yamamoto, T., Matsui, T., Nakafuku, M., Iwamatsu, A., and Kaibuchi, K. (1995). A novel GTPase-activating protein for R-Ras. J. Biol. Chem. *270*, 30557–30561.

Yeaman, C., Grindstaff, K. K., Wright, J. R., and Nelson, W. J. (2001). Sec6/8 complexes on trans-Golgi network and plasma membrane regulate late stages of exocytosis in mammalian cells. J. Cell Biol. *155*, 593–604.

Zacharias, D. A., Violin, J. D., Newton, A. C., and Tsien, R. Y. (2002). Partitioning of lipid-modified monomeric GFPs into membrane microdomains of live cells. Science *296*, 913–916.

Zhang, X. M., Ellis, S., Sriratana, A., Mitchell, C. A., and Rowe, T. (2004). Sec15 is an effector for the Rab11 GTPase in mammalian cells. J. Biol. Chem. *279*, 43027–43034.

Zhang, Z., Vuori, K., Wang, H., Reed, J. C., and Ruoslahti, E. (1996). Integrin activation by R-ras. Cell *85*, 61–69.

Increased Endoplasmic Reticulum Stress in Atherosclerotic Plaques Associated With Acute Coronary Syndrome

Masafumi Myoishi, MD; Hiroyuki Hao, MD, PhD; Tetsuo Minamino, MD, PhD; Kouki Watanabe, MD, PhD; Kensaku Nishihira, MD, PhD; Kinta Hatakeyama, MD, PhD; Yujiro Asada, MD, PhD; Ken-ichiro Okada, MD, PhD; Hatsue Ishibashi-Ueda, MD, PhD; Giulio Gabbiani, MD, PhD; Marie-Luce Bochaton-Piallat, PhD; Naoki Mochizuki, MD, PhD; Masafumi Kitakaze, MD, PhD

Background—The endoplasmic reticulum (ER) responds to various stresses by upregulation of ER chaperones, but prolonged ER stress eventually causes apoptosis. Although apoptosis is considered to be essential for the progression and rupture of atherosclerotic plaques, the influence of ER stress and apoptosis on rupture of unstable coronary plaques remains unclear.

Methods and Results—Coronary artery segments were obtained at autopsy from 71 patients, and atherectomy specimens were obtained from 40 patients. Smooth muscle cells and macrophages in the fibrous caps of thin-cap atheroma and ruptured plaques, but not in the fibrous caps of thick-cap atheroma and fibrous plaques, showed a marked increase of ER chaperone expression and apoptotic cells. ER chaperones also showed higher expression in atherectomy specimens from patients with unstable angina pectoris than in specimens from those with stable angina. Expression of 7-ketocholesterol was increased in the fibrous caps of thin-cap atheroma compared with thick-cap atheroma. Treatment of cultured coronary artery smooth muscle cells or THP-1 cells with 7-ketocholesterol induced upregulation of ER chaperones and apoptosis, whereas these changes were prevented by antioxidants. We also investigated possible signaling pathways for ER-initiated apoptosis and found that the CHOP (a transcription factor induced by ER stress)-dependent pathway was activated in unstable plaques. In addition, knockdown of CHOP expression by small interfering RNA decreased ER stress-dependent death of cultured coronary artery smooth muscle cells and THP-1 cells.

Conclusions—Increased ER stress occurs in unstable plaques. Our findings suggest that ER stress-induced apoptosis of smooth muscle cells and macrophages may contribute to plaque vulnerability. (***Circulation.* 2007;116:1226-1233.**)

Key Words: apoptosis ■ plaque ■ myocardial infarction ■ endoplasmic reticulum

Most of the acute clinical manifestations of coronary atherosclerosis result from plaque rupture that triggers thrombosis and vessel occlusion, producing the acute coronary syndrome (ACS).[1–3] Previous reports have shown that apoptosis affects all of the types of cells residing within atherosclerotic plaques, including smooth muscle cells (SMCs) and macrophages,[4,5] with oxidized low-density lipoprotein and several inflammatory factors being known to induce apoptosis.[6,7] The number of apoptotic cells depends on the plaque stage and is generally higher in more advanced plaques.[6,8] SMCs synthesize most of the interstitial collagen that stabilizes the fibrous cap of a plaque.[4,7] Therefore, excessive apoptosis of SMCs in the fibrous cap may compromise plaque integrity and render it vulnerable to proteolytic attack by inflammatory cells, leading to plaque rupture.[4,7] Apoptotic macrophages are more frequent at sites of plaque rupture than in areas where the fibrous cap remains intact.[9] A decrease in macrophages would reduce the scavenging of apoptotic SMCs and macrophages, allowing the cells to undergo secondary necrosis, thereby increasing thrombogenicity of the plaque.[10]

Editorial p 1214
Clinical Perspective p 1233

The endoplasmic reticulum (ER) is 1 of the largest cellular organelles and has multiple functions, such as regulating the folding of proteins.[11,12] Various stimuli cause ER stress,

Received December 10, 2006; accepted July 6, 2007.

From the Departments of Cardiovascular Medicine (M.M., M.K.), Structural Analysis (M.M., N.M.), and Pathology (H.H., H.I.-U.), National Cardiovascular Center, Suita, Osaka, Japan; Department of Surgical Pathology (H.H.), Hyogo College of Medicine, Nishinomiya, Hyogo, Japan; Departments of Bioregulatory Medicine (M.M.) and Cardiovascular Medicine (T.M., K.-i.O.), Osaka University Graduate School of Medicine, Suita, Osaka, Japan; Division of Cardiology (K.W.), Uwajima City Hospital, Uwajima, Ehime, Japan; Department of Pathology (K.N., K.H., Y.A.), Faculty of Medicine, University of Miyazaki, Miyazaki, Japan; and Department of Pathology and Immunology (G.G., M.-L.B.-P.), University of Geneva–CMU, Geneva, Switzerland.

The online-only Data Supplement, consisting of expanded Methods, tables, and figures, is available with this article at http://circ.ahajournals.org/cgi/content/full/CIRCULATIONAHA.106.682054/DC1.

Correspondence to Masafumi Kitakaze, MD, PhD, Department of Cardiovascular Medicine, National Cardiovascular Center, Suita, Osaka 565-8565, Japan. E-mail kitakaze@zf6.so-net.ne.jp

Circulation **is available at http://circ.ahajournals.org** **DOI: 10.1161/CIRCULATIONAHA.106.682054**

including ischemia, hypoxia, heat shock, mutation, increased protein synthesis, and reactive oxygen species, all of which can potentially lead to ER dysfunction.[11,12] In response to ER stress, there is marked upregulation of various ER chaperones, such as the 94-kDa glucose-regulated protein (GRP94) or GRP78 that stabilizes protein folding.[11,13,14] When the ER becomes overloaded with misfolded proteins, the unfolded protein response (UPR) occurs to enhance cell survival.[15] However, prolonged ER stress can trigger apoptotic cell death, which is promoted by transcriptional induction of C/EBP homologous protein (CHOP) and/or by the activation of c-JUN NH_2-terminal kinase (JNK)– and/or caspase-12–dependent pathways.[16] In support of this concept, our investigation of the effects of prolonged ER stress on hypertrophic and failing hearts revealed that apoptosis of cardiac myocytes was induced via activation of CHOP, an ER-specific proapoptotic factor.[17] An important role of ER-initiated cell death pathways has also been demonstrated in several diseases, including diabetes mellitus,[16] neurodegenerative conditions,[18] and ischemia.[19]

Oxidation of low-density lipoprotein plays a significant pathogenetic role in atherosclerosis.[6,7,20] In cultured peritoneal macrophages, excessive accumulation of free cholesterol (induced by acetyl low-density lipoprotein with an acyl-CoA:cholesterol acyltransferase [ACAT] inhibitor) initiates ER stress, increases CHOP expression, and leads to apoptosis.[21] Studies of $apoE^{-/-}$ mice also support the relevance of ER stress to macrophage apoptosis and to enlargement of the necrotic core in advanced atherosclerotic plaques.[22,23] However, it is still unclear whether ER stress and UPR activation have a role in plaque rupture. Unfortunately, the absence of a suitable animal model has greatly hindered investigation of the molecular mechanisms of plaque rupture and evaluation of the effects of ER stress in vivo.[24,25]

In the present study, we examined histological sections from atherosclerotic coronary artery lesions obtained at autopsy or after directional coronary atherectomy (DCA) to investigate markers of ER stress/UPR activation and apoptotic cell death. Oxysterols such as 7-ketocholesterol (7-KC) have been reported to be partially responsible for the cytotoxicity of oxidized low-density lipoprotein.[26,27] Exposure of cultured human SMCs to 7-KC induces the UPR and promotes apoptotic cell death,[28] so we investigated 7-KC expression in plaque specimens by immunohistochemistry. We also examined whether 7-KC could activate ER stress using cultured human coronary artery SMCs (CASMCs) and a monocyte cell line (THP-1). Furthermore, we investigated the possible signaling pathways for ER-initiated apoptosis, and we found that the CHOP (a transcription factor induced by ER stress)-dependent pathway was activated in unstable plaques, whereas knockdown of CHOP expression by small interfering RNA (siRNA) decreased ER stress-dependent death of cultured CASMCs and THP-1 cells.

Methods

Coronary Artery Specimens

Two different sets of specimens were obtained under a protocol approved by the Institutional Review Board of the National Cardiovascular Center and Miyazaki University. The first set of specimens was obtained at autopsy, and the second set was obtained by DCA. Classification of the histology of the lesions in autopsy specimens was done morphologically, as described previously (Table 1).[29–31] Demographic data for the study population are presented in Table I of the Data Supplement.

TABLE 1. Human Coronary Specimens (Autopsy; n=71)

Histological Classification of Lesions	No. of Specimens	AHA Classification
No. of specimens obtained at autopsy	152	...
Diffuse intimal thickening (normal)	21	Type I
Fibrous plaques (fibrous)	48	Type Vc
Thick-cap atheroma (thick)	51	Type Va
Thin-cap atheroma (thin)	15	Type Va
Ruptured plaques (ruptured)	17	Type VI

AHA Classification indicates American Heart Association histological criteria.[30,31]

In brief, 152 coronary artery segments were obtained at autopsy from 71 patients, including 17 consecutive patients who experienced fatal ACS without percutaneous coronary intervention and 54 consecutive patients with noncardiac death. The major coronary arteries and their branches were cut transversely at ≈5-mm intervals, and 17 ruptured plaques were detected in the 17 ACS patients (ruptured: AHA type VI, n=17). The remaining 33 patients with noncardiac death and the 17 ACS patients also had advanced unruptured plaques (≥75% cross-sectional luminal narrowing), and we assessed each segment at the narrowest point (n=114). The advanced atherosclerotic unruptured plaques were additionally divided into fibrous plaques (fibrous: fibrocellular tissue was the predominant component, and the lipid core was inconspicuous or absent; AHA type Vc, n=48), thick-cap atheroma (thick: a lipid core covered by a fibrous cap >65-μm thick; AHA type Va, n=51), and thin-cap atheroma (thin: a lipid-rich core covered by a fibrous cap <65-μm thick[32]; AHA type Va, n=15). Another 21 patients with noncardiac death who had no advanced unruptured plaques and normal coronary arteries that only showed diffuse intimal thickening (normal: AHA type I, n=21) were used as a control group.

We performed a morphological analysis of multiple lesions (n=152) obtained at autopsy from 71 patients (Figure 1). The supplementary analyses included pairwise comparison of unruptured and ruptured plaques from each heart of each patient with ACS (Data Supplement Figure I) and investigation of the correlation between traditional cardiovascular risk factors and ER stress (Data Supplement Table II and Figure III). These supplementary analyses were based on representative data from each patient. (Details of the methods used to perform the supplementary analyses are included in the expanded Methods section in the Data Supplement.)

Forty DCA specimens were obtained from 40 patients who were treated for stable angina pectoris (SAP; n=20) or unstable angina pectoris (UAP; n=20). One DCA specimen was obtained per patient, and these specimens were classified on the basis of the clinical situation at the time of DCA (Table 2). These specimens were fixed in 4% paraformaldehyde for 6 hours at 4°C and then embedded in paraffin.

Immunohistochemistry

Serial sections were examined by immunohistochemistry, as described previously.[17] In brief, sections were deparaffinized, and endogenous peroxidase activity was blocked by incubation with 0.3% H_2O_2 in methanol for 30 minutes. For some antibodies, antigen retrieval was performed as specified below. After blocking with 3% normal bovine serum albumin, sections were incubated with the primary antibody overnight at 4°C. KDEL (Lys-Asp-Glu-Leu) antibody, which recognizes both GRP78 and GRP94, was purchased from Stressgen (San Diego, Calif) and was used at a dilution of 1:2000. Anti-CHOP antibody was obtained from Santa Cruz Biotechnology (Santa Cruz, Calif) and was applied at a dilution of 1:600

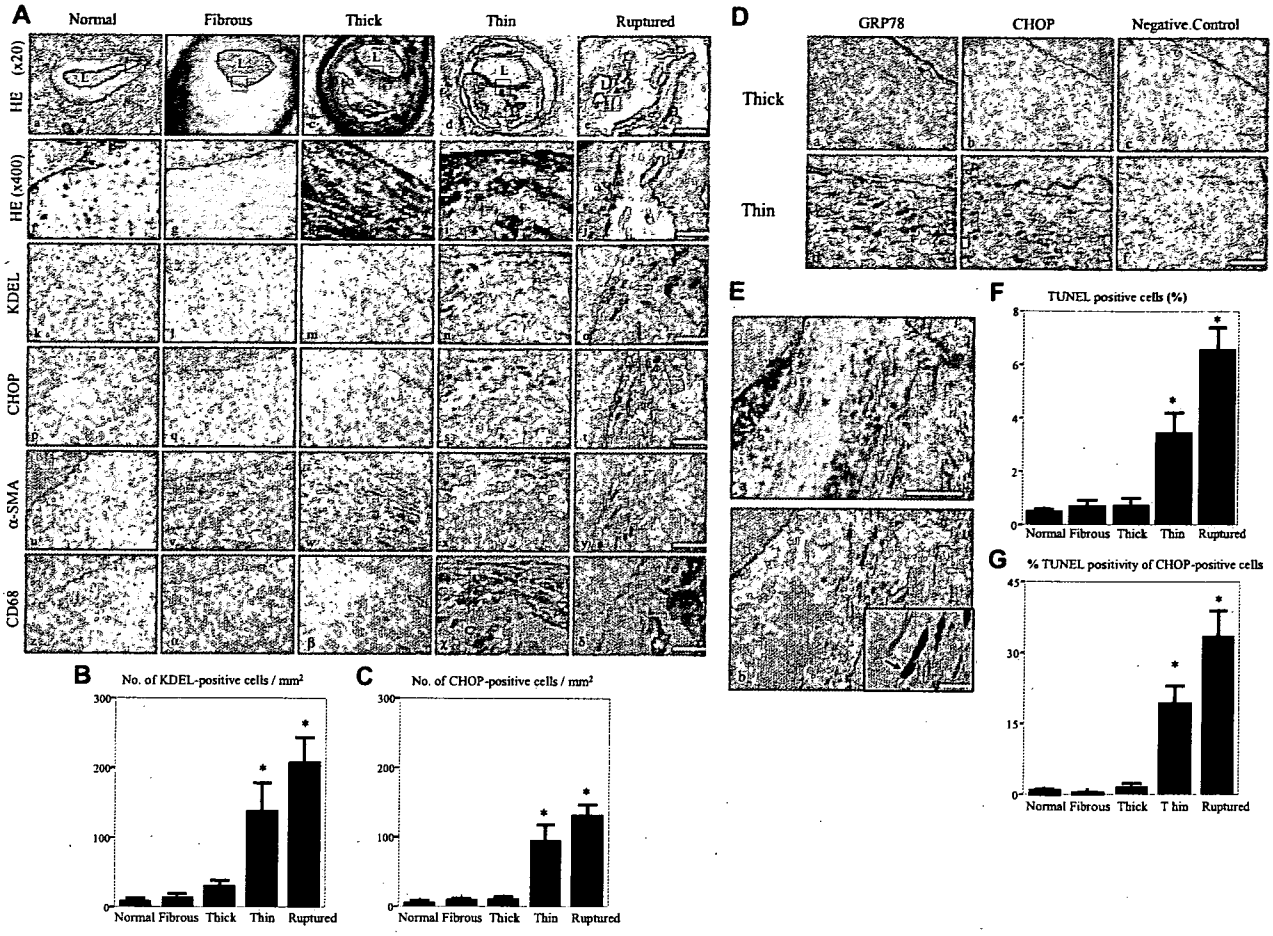

Figure 1. Induction of ER chaperones and death signals in coronary artery plaques obtained at autopsy. A, Comparison of hematoxylin-eosin (HE) staining, KDEL immunostaining, and CHOP immunostaining of normal arteries (n=14), fibrous plaques (n=48), thick-cap atheroma (n=51), thin-cap atheroma (n=15), and ruptured plaques (n=17) obtained at autopsy from 71 patients. Representative HE-stained low-power micrographs from each group (a through e). L indicates the lumen, and the arrow shows the site of plaque rupture. The parts of the intima (a) and fibrous cap (b through e) indicated by boxes are shown at a higher magnification in panels f through j. Panels k through o show KDEL immunostaining. Panels p through t show CHOP immunostaining. Panels u through y show α-smooth muscle actin (α-SMA) immunostaining. Panels z through δ show CD68 immunostaining. B and C, The number of KDEL-positive (B) and CHOP-positive (C) cells. The absolute number per square millimeter is shown for the media of a normal artery and for the fibrous caps of fibrous plaques, thick-cap atheroma, thin-cap atheroma, and ruptured plaques (B, C). D, ISH analysis of GRP78 (a, d), CHOP (b, e), and negative control (c, f) mRNA expression in thick- and thin-cap atheromas. E, Comparison of HE staining (a) with double immunostaining (b). Colocalization of CHOP (red) with TUNEL-positive cells (brown) in the cap of a ruptured plaque. The area indicated by asterisks is shown at a higher magnification in the inset. Arrows show CHOP and TUNEL double-positive cells. F and G, Percentage of TUNEL-positive cells (F) and percentage of TUNEL-positive cells among CHOP-positive cells (G) in the fibrous cap. Scale bars represent 1 mm (A, a through e), 50 μm (A, f through δ, D, and E), and 20 μm (E, in inset). *$P<0.05$ vs normal plaque.

after antigen retrieval by incubation for 10 minutes at room temperature in 5 μg/mL proteinase K. Anti-phospho-c-JUN NH_2-terminal kinase antibody was used to detect c-JUN kinase (JNK), which is involved in the UPR.[16] It was obtained from Cell Signaling (Danvers, Mass) and was applied at a dilution of 1:100 after heat retrieval for 15 minutes at a sub-boiling temperature in 1 mmol/L EDTA (pH 8.0). Colon carcinoma sections were stained with anti-phospho-JNK antibody as a positive control. Anti-α-smooth muscle actin antibody and anti-human CD68 antibody (DAKO, Glostrup, Denmark) were used to identify SMCs and macrophages, respectively, and were used at a dilution of 1:200. The EnVision kit (DAKO) was then used for immunostaining. Application of the KDEL antibody or the CHOP antibody after preincubation with each synthetic peptide used for immunization (KDEL: synthetic peptide SEKDEL, 10 μg/mL, Tore Bio, CHOP peptide: 10 μg/mL, Santa Cruz Biotechnology) resulted in no detectable signals, demonstrating the specificity of the antibody (Data Supplement Figure II).

TABLE 2. Human Coronary Specimens (Atherectomy; n=40)

Origin and Classification of Plaques	No. of Specimens
SAP	20
UAP	20

Terminal dUTP Nick End-Labeling Method and Double Immunohistochemistry

Cells undergoing apoptosis were identified by the terminal dUTP nick end-labeling (TUNEL) method with the ApopTag In Situ Apoptosis Detection Kit (Chemicon, Temecula, Calif), as described previously.[8] For simultaneous identification of CHOP and TUNEL immunoreactivity, double immunostaining of specimens was performed. First, the TUNEL method was performed with an ApopTag

kit, and then CHOP was detected with an alkaline phosphatase–labeled secondary antibody with NewFukusin (DAKO).

In Situ Hybridization

Digoxigenin-labeled cRNA probes and the negative control (LNE120) were purchased from Direct Communications Inc (Hirosaki, Japan), and the sequences were as follows: GRP78: 5′-UGGAAUUCGAGUCGAGCCACCAACAAGAACAAUUUCAUCAAUAUCAGACUUCUUCAAAUCAGAAUCUUCCAACACUUUCUGGACGGGCUUCAUAGUAGACCGGAACAGAUCCA UGUUGAG-3′; CHOP: 5′-AUGCUCCCAAUUGUUCAUGCUUGGUGCAGAUUCACCAUUCGGUCAAUCAGAGCUCGGCGAGUCGCCUCUACUUCCCUGGUCAGGCGCUCGAUUUCCUGCUUGAGCCGUUCAUUCUCUUC-3′. In situ hybridization (ISH) was performed as described previously[33] with a Microprobe manual staining system (Fisher Scientific, Pittsburgh, Pa). In brief, hybridization of the probes (1 μg/mL) was performed for 120 minutes at 50°C, and then anti-digoxigenin-Ap (x250, Roche, Basel, Switzerland), as the secondary antibody, and NBT/BCIP stock solution (×50, Roche) were added.

7-KC Staining

Snap-frozen samples were obtained from 12 patients, comprising 6 with thick-cap atheroma and 6 with thin-cap atheroma. Frozen sections were fixed in 10% neutral-buffered formalin for 1 hour at room temperature. After blocking with 3% normal bovine serum albumin, the sections were incubated overnight at 4°C with anti-7-KC antibody (Nikken Seil Corporation, Fukuroi, Japan) at a dilution of 1:100, followed by incubation with an EnVision kit for 30 minutes.

Statistical Analysis

Data are expressed as mean±SEM. For the autopsy study of multiple lesions from many patients (Figure 1), statistical analysis was performed with the Kruskal–Wallis *H* test and a post hoc Mann-Whitney *U* test. For the DCA specimens, statistical analysis was performed with the Mann-Whitney *U* test. Experiments with cultured cells were performed at least 3 times each. Data obtained with cultured cells were analyzed statistically by the unpaired Student *t* test or ANOVA, followed by the Bonferroni test. Comparison of categorical variables was done with Fisher exact test. In all analyses, $P<0.05$ was accepted as statistically significant. The expanded Methods section, covering supplementary data and in vitro studies is included as an online-only Data Supplement.

The authors had full access to and take full responsibility for the integrity of the data. All authors have read and agree to the manuscript as written.

Results

Upregulation of ER Chaperones and Apoptosis in the Fibrous Caps of Thin-Cap Atheroma and Ruptured Plaques

In the fibrous caps of thin-cap atheroma and ruptured plaques, KDEL and CHOP immunostaining showed a marked increase compared with the level of staining in the fibrous caps of thick-cap atheroma and fibrous plaques (Figure 1A k through t, Figure 1B, and Figure 1C). KDEL-positive cells were more numerous than CHOP-positive cells in the fibrous caps of thin-cap atheroma and ruptured plaques. Most of the CHOP-positive cells also expressed KDEL, as shown by staining of serial sections. In the same hearts of the ACS patients, there was a significant difference of KDEL- and CHOP-positive cells between the unruptured and ruptured plaques (Data Supplement Figure I). We also assessed ER chaperone (GRP78) and CHOP expression at the mRNA level by ISH (Figure 1D). Furthermore, we confirmed that the KDEL- and CHOP-positive cells were SMCs or macrophages by immunostaining of serial sections with anti α-smooth muscle actin and anti-CD68, respectively (Figure 1A, u through δ). In the fibrous caps of thin-cap atheroma and ruptured plaques, colocalization of CHOP immunoreactivity with TUNEL-positive cells was observed by double immunostaining (Figure 1E). The percentage of TUNEL-positive cells (Figure 1F) and the percentage of TUNEL-positive cells among CHOP-positive cells (Figure 1G) were increased compared with the findings in other specimens. Immunostaining for phospho-JNK, which is a proapoptotic factor involved in ER stress, revealed no immunoreactivity in the fibrous caps of thick, thin, or ruptured plaques (data not shown). In normal coronary artery specimens with diffuse intimal thickening (Figure 1A, k and p), there was no KDEL or CHOP positivity. In the region around the necrotic core of advanced plaques, KDEL positivity was only observed in macrophages. There was no significant difference in the number of KDEL-positive cells within the area surrounding the necrotic core of thick-cap atheromas (726±88/mm^2), thin-cap atheromas (741±52/mm^2), and ruptured plaques (651±102/mm^2).

Upregulation of ER Stress in Atherectomy Specimens From Patients With UAP

To estimate the activation of ER stress related to the clinical situation, we examined histological sections obtained at DCA. Morphometric analysis demonstrated that the number of KDEL- and CHOP-positive cells was significantly higher in patients with UAP than in patients with SAP ($P<0.05$; Figures 2A, 2B, and 2C). The KDEL- and CHOP-positive cells were confirmed to be SMCs and macrophages (Figure 2A). When ER chaperone (GRP78) and CHOP mRNA levels were analyzed by quantitative reverse-transcription polymerase chain reaction or ISH, GRP78 expression was increased in patients with UAP ($P=0.14$; Figure 2D), whereas CHOP expression was significantly higher in UAP patients than in SAP patients ($P<0.05$; Figure 2E). On the other hand, both GRP78 and CHOP were significantly increased according to ISH (Figure 2F), but we could not confirm a significant increase of GRP78 by reverse-transcription polymerase chain reaction. This may have been because the number of fresh DCA specimens was too low.

Immunohistochemical Detection of 7-KC in the Fibrous Caps of Atherosclerotic Plaques

To explore the likely molecular mechanism of activation of ER stress and the mechanistic link to apoptosis, we investigated plaque lipids by staining frozen coronary artery sections with anti-7-KC antibody (Figure 3), and the in vitro studies were performed (Figure 4). Immunoreactivity for 7-KC was increased in the fibrous caps of thin-cap atheroma, whereas no immunoreactivity was detected in the fibrous caps of thick-cap atheroma (Figure 3). In the region around the lipid core, however, 7-KC immunoreactivity was visible in both types of atheroma (Figure 3).

Upregulation of ER Chaperones, CHOP, and Apoptosis by 7-KC and Effects of CHOP Knockdown by siRNA in CASMCs or THP-1 Cells

Exposure of cells to 7-KC increased the expression of GRP78 and CHOP mRNA, whereas this increase was prevented by

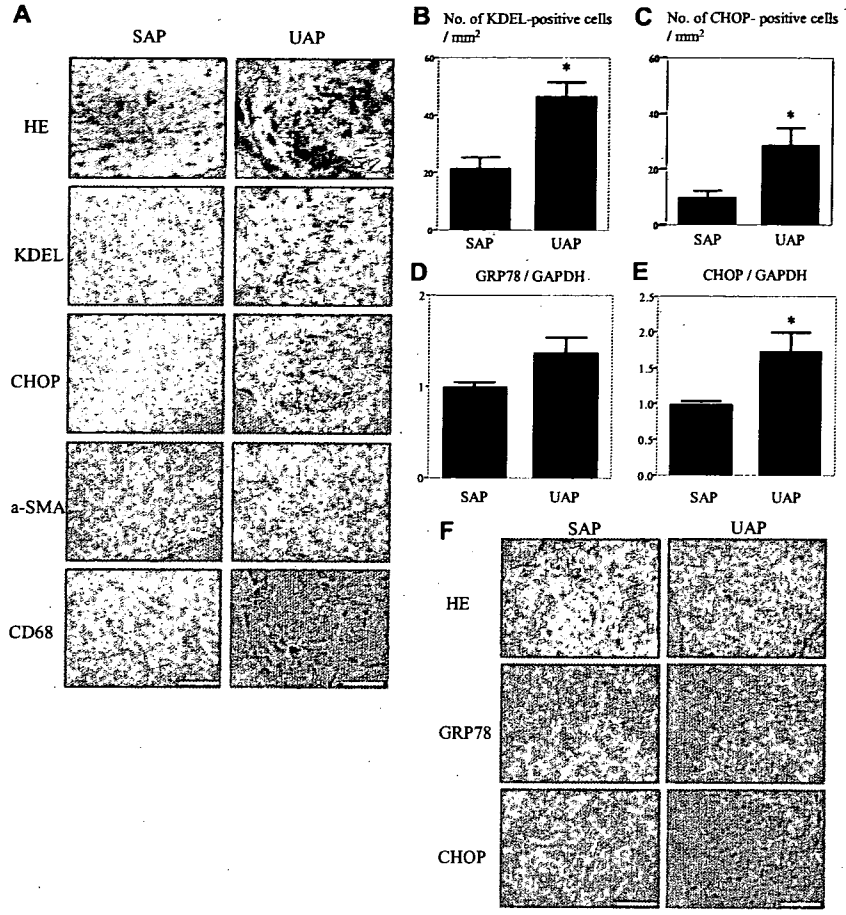

Figure 2. Induction of ER chaperones and death signals in atherectomy specimens obtained from the culprit lesions of patients with UAP. A, Comparison of hematoxylin-eosin (HE) staining with KDEL, CHOP, α-smooth muscle actin (a-SMA), and CD68 immunostaining of the serial sections of 32 atherectomy specimens obtained from patients with SAP (n=16) or UAP (n=16). B and C, Number of KDEL-positive (B) and CHOP-positive (C) cells per square millimeter. D and E, Comparison of GRP78 and CHOP expression normalized for GAPDH in 8 specimens from patients with SAP (n=4) or UAP (n=4) by quantitative reverse-transcription polymerase chain reaction. F, HE staining and ISH analysis of GRP78 (a, d) and CHOP (b, e) mRNA expression in specimens from SAP patients (n=6) or UAP patients (n=6). Scale bar represents 50 μm. *P<0.05 vs SAP.

the antioxidants *N*-acetylcysteine or glutathione (Figure 4A). We observed intracellular production of reactive oxygen species after exposure to 7-KC, whereas glutathione reduced reactive oxygen species production (Figure 4B). We also examined the effects of 7-KC on apoptosis of CASMCs and THP-1 cells (Figure 4C). Treatment with 7-KC increased FITC-annexin and propidium iodide staining in a dose-dependent (Figure 4C, b and c) and time-dependent (data not shown) manner. Treatment of CASMCs and THP-1 cells with 7-KC for 24 hours also induced apoptosis along with the induction of ER chaperones and CHOP at the protein level (Figure 4D). When CASMCs and THP-1 cells were simultaneously incubated with 7-KC and *N*-acetylcysteine or glutathione, both antioxidants reduced the induction of ER chaperones (Figure 4D). Quantitative analysis revealed that most of the CHOP-positive cells coexpressed KDEL (88.2% of CHOP-positive CASMCs and 72.7% of CHOP-positive THP-1 cells; P<0.05, Fisher's exact test), whereas there were few KDEL-negative and CHOP-positive cells, which suggests that CHOP was involved in the mediation of ER-initiated signaling (Figure 4D, c and d). Treatment of THP-1 cells with 7-KC induced CHOP, whereas 2 different siRNAs targeting CHOP caused the knockdown of CHOP expression (Figure 4E, a). Knockdown of CHOP expression by siRNA decreased the number of TUNEL-positive THP-1 cells after exposure to 7-KC (Figure 4E, b and d). Similarly, the knockdown of CHOP expression by siRNA decreased the number of TUNEL-positive CASMCs after exposure to 7-KC (Figure 4E, c).

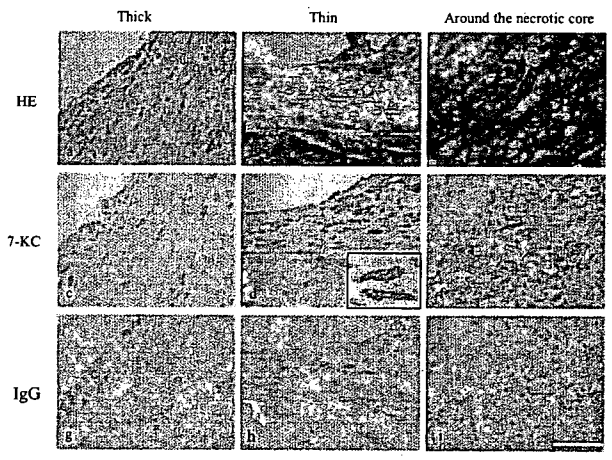

Figure 3. Immunohistochemical detection of 7-KC in the fibrous cap of thin-cap atheroma. Comparison of hematoxylin-eosin (HE) staining with 7-KC or IgG immunostaining in the fibrous caps of thick-cap atheroma (n=6) and thin-cap atheroma (n=6), as well as around the necrotic core of thick-cap atheroma. 7-KC immunostaining is shown at a higher magnification in the inset. Scale bar represents 50 μm.

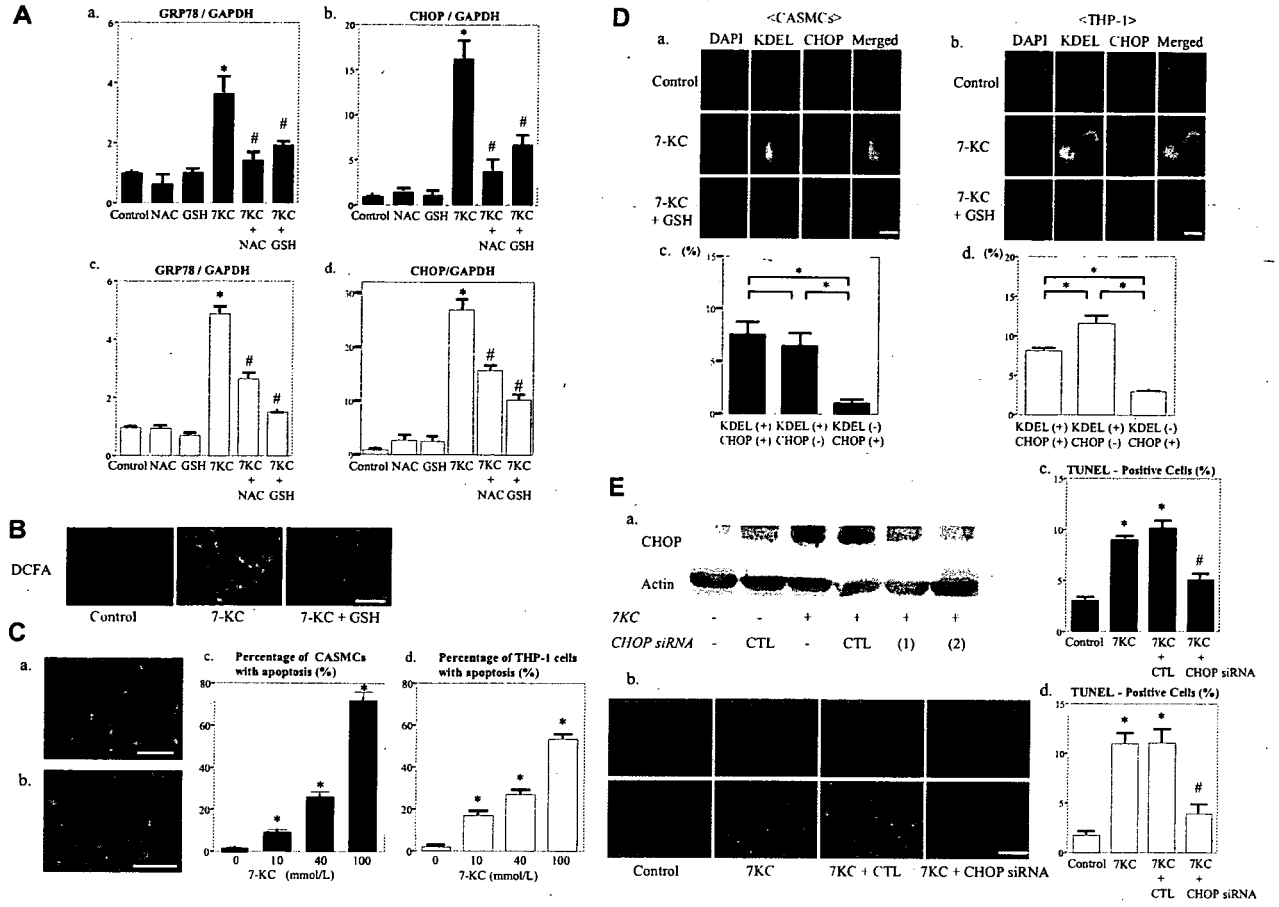

Figure 4. Upregulation of ER chaperones, CHOP, and apoptosis by exposure to 7-KC and effect of CHOP knockdown by siRNA in cultured CASMCs or THP-1 cells. A, Comparison of GRP78 and CHOP expression normalized for GAPDH by quantitative reverse-transcription polymerase chain reaction. CASMCs or THP-1 cells were incubated with 7-KC (80 mmol/L) in the absence or presence of *N*-acetylcysteine (NAC) or glutathione (GSH) for 12 hours. B, Measurement of reactive oxygen species (ROS) generation after exposure to 7-KC and 2′, 7′-dichlorofluorescin diacetate (DCFH-DA) in the absence or presence of GSH for 12 hours. C, FITC-annexin V and propidium iodide staining for apoptosis of CASMCs and THP-1 cells incubated with 7-KC (a). Exposure to 7-KC induced apoptosis of CASMCs (b) and THP-1 cells (c) in a dose-dependent manner. D, KDEL and CHOP staining of CASMCs (a) and THP-1 cells (b) after incubation with 7-KC in the absence or presence of GSH for 24 hours; c and d, quantitative analysis of immunohistochemical staining of CASMCs (c) and THP-1 cells (d). E, Western blotting for CHOP after exposure to 7-KC with or without CHOP siRNA (a). TUNEL staining of THP-1 cells (b) and quantitative analysis of TUNEL-positive CASMCs (c) and THP-1 cells (d). CTL indicates the nonsilenced control. Scale bars represent 50 μm (B, C, and E) and 20 μm (D). $^*P<0.05$ vs control (A, C, and E). $\#P<0.05$ vs treatment with 7-KC (E). Experiments were performed at least 3 times. The data are expressed as mean±SEM. The immunofluorescent staining and Western blotting data are representative of at least 3 independent experiments.

Discussion

The present study revealed a marked increase of ER chaperone expression, CHOP expression, and apoptosis in the fibrous caps of thin-cap atheroma or ruptured plaques, as well as in atherectomy specimens from UAP patients, which suggests that ER stress may play a role in the progression of plaque vulnerability and the occurrence of acute complications of coronary atherosclerosis in humans. Because of the inherent limitations of an autopsy study, we could not exclude the possibility that UPR activation occurred after plaque rupture. Previous reports have shown that ER chaperones, such as GRP78 or GRP94, may have a protective effect against ischemia/reperfusion injury.[34] However, the presence of apoptotic changes in the thin-cap atheroma of the patients with noncardiac death suggested that the findings we observed in ruptured plaques represented the evolution of such changes in the thin-cap atheroma rather than being secondary to plaque rupture or ischemia/reperfusion injury. Only specimens from patients without percutaneous coronary intervention were studied, to exclude the influence of this intervention. We also observed an increase of ER stress-related changes in freshly fixed atherectomy specimens obtained from UAP patients compared with those from SAP patients. This suggests that ER stress activation was related to the clinical situation, and the autopsy specimens were only slightly affected by postmortem protein degradation.

Among the oxysterols, 7-KC is most frequently detected at high levels in atherosclerotic plaques and in the plasma of patients with a high cardiovascular risk.[26,35] To the best of our knowledge, however, 7-KC has not previously been detected in human atherosclerotic coronary artery sections by immunohistochemistry. It has been reported that 7-KC induces the

production of reactive oxygen species, activation of the UPR, and induction of apoptotic death in cultured human SMCs.[28] We demonstrated that the fibrous caps of thin-cap atheroma were immunohistochemically positive for 7-KC, a finding consistent with the increase of ER stress/UPR markers.

Treatment of CASMCs with 7-KC induced ER stress and activation of the UPR, findings that were consistent with the results of a previous study on aortic SMCs,[28] and these changes also occurred in THP-1 cells. This 7-KC–induced cellular damage was prevented by antioxidants (*N*-acetylcysteine and glutathione), which was also consistent with a previous report.[36] Accordingly, the present findings suggest that an increase of ER stress due to 7-KC induces apoptosis of SMCs and macrophages through the production of reactive oxygen species.

ER stress induces apoptosis via the CHOP-, JNK-, and caspase-12–dependent signaling pathways.[16] CHOP is mainly induced at the transcriptional level by ER stress,[12,37] after which its overexpression leads to apoptosis.[11,16,38] CHOP knockout mice show normal development and normal fertility but exhibit less apoptosis in response to ER stress.[16,21] Thus, detection of the induction of CHOP indicates an increase of ER-initiated apoptosis. Although the direct transcriptional target of CHOP has not been found,[39] the Bcl-2 pathway may be involved in the downstream connection between CHOP and apoptosis.[28,39] Caspase-12 is only activated by ER stress.[13,16,18] Although caspase-12 has been cloned in mice and rats, it is not yet possible to explore the role of this caspase in humans.[40] JNK is 1 of the stress-activated protein kinases that has been shown to induce apoptosis in response to ER stress.[13,16] We demonstrated that TUNEL-positive SMCs and macrophages were significantly increased in the fibrous cap, with CHOP (but not JNK) being induced simultaneously. Treatment of CASMCs or THP-1 cells with 7-KC induced CHOP, whereas knockdown of CHOP expression by siRNA led to a decrease of TUNEL-positive cells after exposure to 7-KC. Because CHOP is a transcription factor that specifically mediates ER-initiated apoptosis, the induction of CHOP in ruptured and unstable plaques supports the activation of ER-initiated apoptosis. However, our autopsy study could not exclude the possibility that the cells underwent apoptosis independently of CHOP, whereas the TUNEL assay gave false-positive results in the clinical specimens.

Unfortunately, we could not confirm whether or not the relationship between thinning of the fibrous cap and ER stress was causative because of the lack of a suitable animal model of plaque rupture. On the other hand, together with the present finding that 7-KC induced ER stress, the possibility that ER stress causes plaque vulnerability is also supported by the following reports. In cultured peritoneal macrophages, excessive accumulation of free cholesterol has been found to initiate ER stress, increase CHOP expression, and increase apoptosis.[21] Moreover, in vivo studies with apoE$^{-/-}$ mice have shown that lesional necrosis can be diminished by a decrease in the cholesterol level.[22] In addition, the present study demonstrated that expression of ER chaperones was upregulated to a similar extent in macrophages surrounding the necrotic cores of thick-cap atheroma, thin-cap atheroma, and ruptured plaques, which suggests that ER stress may contribute to the progression of plaque vulnerability by inducing macrophage apoptosis.

In conclusion, the present findings support the possibility that ER stress and/or the UPR induces apoptosis of SMCs and macrophages, thus increasing the vulnerability of coronary artery plaques, which may lead to ACS and a fatal outcome in patients with coronary artery disease.

Acknowledgments

We thank Akiko Ogai, Tomoko Morita, and Kazuyoshi Masuda for their technical assistance and Akiko Kada and Nobuo Shirahashi for their statistical advice.

Sources of Funding

The present study was supported by a grant from the Japan Cardiovascular Research Foundation and a research grant for cardiovascular disease (14C-4) from the Japanese Ministry of Health, Labor and Welfare.

Disclosures

None.

References

1. Fuster V. Lewis A. Conner Memorial Lecture: mechanisms leading to myocardial infarction: insights from studies of vascular biology. *Circulation.* 1994;90:2126–2146.
2. Lee RT, Libby P. The unstable atheroma. *Arterioscler Thromb Vasc Biol.* 1997;17:1859–1867.
3. Falk E, Shah PK, Fuster V. Coronary plaque disruption. *Circulation.* 1995;92:657–671.
4. Bennett MR. Apoptosis of vascular smooth muscle cells in vascular remodeling and atherosclerotic plaque rupture. *Cardiovasc Res.* 1999;41:361–368.
5. Bjorkerud S, Bjorkerud B. Apoptosis is abundant in human atherosclerotic lesions, especially in inflammatory cells (macrophages and T cells), and may contribute to the accumulation of gruel and plaque instability. *Am J Pathol.* 1996;149:367–380.
6. Littlewood TD, Bennett MR. Apoptotic cell death in atherosclerosis. *Curr Opin Lipidol.* 2003;14:469–475.
7. Lindstedt KA, Leskinen MJ, Kovanen PT. Proteolysis of the pericellular matrix: a novel element determining cell survival and death in the pathogenesis of plaque erosion and rupture. *Arterioscler Thromb Vasc Biol.* 2004;24:1350–1358.
8. Kockx MM, De Meyer GR, Muhring J, Jacob W, Bult H, Herman AG. Apoptosis and related proteins in different stages of human atherosclerotic plaques. *Circulation.* 1998;97:2307–2315.
9. Kolodgie FD, Narula J, Burke AP, Haider N, Farb A, Hui-Liang Y, Smialek J, Virmani R. Localization of apoptotic macrophages at the site of plaque rupture in sudden coronary death. *Am J Pathol.* 2000;157:1259–1268.
10. Stoneman V, Bennet MR. Role of apoptosis in atherosclerosis and its therapeutic implications. *Clin Sci.* 2004;107:343–354.
11. Kaufman RJ. Stress signaling from the lumen of the endoplasmic reticulum: coordination of gene transcriptional and translational controls. *Genes Dev.* 1999;13:1211–1233.
12. Ron D. Translational control in the endoplasmic reticulum stress response. *J Clin Invest.* 2002;110:1383–1388.
13. Ferri KF, Kroemer G. Organelle-specific initiation of cell death pathways. *Nat Cell Biol.* 2001;3:E255–E263.
14. Patterson C, Cyr D. Welcome to the machine: a cardiologist's introduction to protein folding and degradation. *Circulation.* 2002;106:2741–2746.
15. Mori K. Tripartite management of unfolded proteins in the endoplasmic reticulum. *Cell.* 2000;101:451–454.
16. Oyadomari S, Araki E, Mori M. Endoplasmic reticulum stress-mediated apoptosis in pancreatic beta-cells. *Apoptosis.* 2002;7:335–345.
17. Okada K, Minamino T, Tsukamoto Y, Liao Y, Tsukamoto O, Takashima S, Hirata A, Fujita M, Nagamachi Y, Nakatani T, Yutani C, Ozawa K, Ogawa S, Tomoike H, Hori M, Kitakaze M. Prolonged endoplasmic

reticulum stress in hypertrophic and failing heart after aortic constriction. *Circulation.* 2004;110:705–712.
18. Nakagawa T, Zhu H, Morishima N, Li E, Xu J, Yankner BA, Yuan J. Caspase-12 mediates endoplasmic-reticulum-specific apoptosis and cytotoxicity by amyloid-beta. *Nature.* 2000;403:98–103.
19. Little E, Tocco G, Baudry M, Lee AS, Schreiber SS. Induction of glucose-regulated protein (glucose-regulated protein 78/BiP and glucose-regulated protein 94) and heat shock protein 70 transcripts in the immature rat brain following status epilepticus. *Neuroscience.* 1996;75: 209–219.
20. Ross R. Atherosclerosis: an inflammatory disease. *N Engl J Med.* 1999; 340:115–126.
21. Feng B, Yao PM, Li Y, Devlin CM, Zhang D, Harding HP, Sweeney M, Rong JX, Kuriakose G, Fisher EA, Marks AR, Ron D, Tabas I. The endoplasmic reticulum is the site of cholesterol-induced cytotoxicity in macrophages. *Nat Cell Biol.* 2003;5:781–792.
22. Feng B, Zhang D, Kuriakose G, Devlin CM, Kockx M, Tabas I. Niemann-Pick C heterozygosity confers resistance to lesional necrosis and macrophage apoptosis in murine atherosclerosis. *Proc Natl Acad Sci U S A.* 2003;100:10423–10428.
23. Zhou J, Lhoták S, Hilditch BA, Austin RC. Activation of unfolded protein response occurs at all stages of atherosclerotic lesion development in apolipoprotein E-deficient mice. *Circulation.* 2005;111:1814–1821.
24. Cullen P, Baetta R, Bellosta S, Bernini F, Chinetti G, Cignarella A, von Eckardstein A, Exley A, Goddard M, Hofker M, Hurt-Camejo E, Kanters E, Kovanen P, Lorkowski S, McPheat W, Pentikainen M, Rauterberg J, Ritchie A, Staels B, Weitkamp B, de Winther M; for the MAFAPS Consortium. Rupture of the atherosclerotic plaque: does a good animal model exist? *Arterioscler Thromb Vasc Biol.* 2003;23:535–542.
25. Lutgens E, Suylen R, Faber BC, Gijbels MJ, Eurlings PM, Bijnens AP, Cleutjens KB, Heeneman S, Daemen MJ. Atherosclerotic plaque rupture: local or systemic process? *Arterioscler Thromb Vasc Biol.* 2003;23: 2123–2130.
26. Brown AJ, Jessup W. Oxysterols and atherosclerosis. *Atherosclerosis.* 1999;142:1–28.
27. Bjorkhem I, Diczfalusy U. Oxysterols: friends, foes, or just fellow passengers? *Arterioscler Thromb Vasc Biol.* 2002;22:734–742.
28. Pedruzzi E, Guichard C, Ollivier V, Driss F, Fay M, Prunet C, Marie JC, Pouzet C, Samadi M, Elbim C, O'Dowd Y, Bens M, Vandewalle A, Gougerot-Pocidalo MA, Lizard G, Ogier-Denis E. NAD(P)H oxidase Nox-4 mediates 7-ketocholesterol-induced endoplasmic reticulum stress and apoptosis in human aortic smooth muscle cells. *Mol Cell Biol.* 2004;24:10703–10717.
29. Naruko T, Ueda M, Haze K, van der Wal AC, van der Loos CM, Itoh A, Komatsu R, Ikura Y, Ogami M, Shimada Y, Ehara S, Yoshiyama M, Takeuchi K, Yoshikawa J, Becker AE. Neutrophil infiltration of culprit lesions in acute coronary syndromes. *Circulation.* 2002;106:2894–2900.
30. Stary HC, Chandler AB, Glagov S, Guyton JR, Insull W Jr, Rosenfeld ME, Schaffer A, Schwartz CJ, Wagner WD, Wissler RW. A definition of initial, fatty streak, and intermediate lesions of atherosclerosis. *Arterioscler Thromb.* 1994;14:840–856.
31. Stary HC, Chandler AB, Dinsmore RE, Fuster V, Glagov S, Insull W, Rosenfeld ME, Schwartz CJ, Wagner WD, Wissler RW. A definition of advanced types of atherosclerotic lesions and a histological classification of atherosclerosis. *Arterioscler Thromb Vasc Biol.* 1995;15:1512–1531.
32. Kolodgie FD, Burke AP, Farb A, Gold HK, Yuan J, Narula J, Finn AV, Virmani R. The thin-cap fibroatheroma: a type of vulnerable plaque: the major precursor lesion to acute coronary syndromes. *Curr Opin Cardiol.* 2001;16:285–292.
33. Kuniyasu H, Ukai R, Johnston D, Troncoso P, Fidler IJ, Pettaway CA. The relative mRNA expression levels of matrix metalloproteinase to E-cadherin in prostate biopsy specimens distinguishes organ-confined from advanced prostate cancer at radical prostatectomy. *Clin Cancer Res.* 2003;9:2185–2194.
34. Martindale JJ, Fernandez R, Thuerauf D, Whittaker R, Gude N, Sussman MA, Glembotski CC. Endoplasmic reticulum stress gene induction and protection from ischemia/reperfusion injury in the hearts of transgenic mice with a tamoxifen-regulated form of ATF6. *Circ Res.* 2006;98: 1186–1193.
35. Zhou Q, Wasowicz E, Handler B, Fleischer L, Kummerow FA. An excess concentration of oxysterols in the plasma is cytotoxic to cultured endothelial cells. *Atherosclerosis.* 2000;149:191–197.
36. Lizard G, Gueldry S, Sordet O, Monier S, Athias A, Miguet C, Bessede G, Lemaire S, Solary E, Gambert P. Glutathione is implied in the control of 7-ketocholesterol-induced apoptosis, which is associated with radical oxygen species production. *FASEB J.* 1998;12:1651–1663.
37. Wang XZ, Lawson B, Brewer JW, Zinszner H, Sanjay A, Mi LJ, Boorstein R, Kreibich G, Hendershot LM, Ron D. Signals from the stressed endoplasmic reticulum induce C/EBP-homologous protein (CHOP/GADD153). *Mol Cell Biol.* 1996;16:4273–4280.
38. Barone MV, Crozat A, Tabaee A, Philipson L, Ron D. CHOP (GADD153) and its oncogenic variant, TLSCHOP, have opposing effects on the induction of G1/S arrest. *Genes Dev.* 1994;8:453–464.
39. Oyadomari S, Mori M. Roles of CHOP/GADD153 in endoplasmic reticulum stress. *Cell Death Differ.* 2004;11:381–389.
40. Fischer H, Koenig U, Eckhart L, Tschachler E. Human caspase 12 has acquired deleterious mutations. *Biochem Biophys Res Commun.* 2002; 293:722–772.

CLINICAL PERSPECTIVE

Most of the acute clinical manifestations of coronary atherosclerosis result from plaque rupture that produces the acute coronary syndrome, and apoptosis is considered to be essential for plaque rupture. The endoplasmic reticulum (ER) is 1 of the largest cellular organelles and has multiple functions, such as regulating the folding of proteins. Various stimuli cause ER stress, including ischemia, heat shock, mutation, increased protein synthesis, and reactive oxygen species, all of which can potentially lead to ER dysfunction. The ER responds to stresses by upregulation of ER chaperones, but prolonged ER stress eventually causes apoptosis. However, the influence of ER stress and apoptosis on rupture of unstable coronary plaques remains unclear. We examined histological sections from coronary artery segments obtained at autopsy from 71 patients and atherectomy specimens obtained from 40 patients. Smooth muscle cells and macrophages in the fibrous caps of thin-cap atheroma and ruptured plaques showed a marked increase of ER chaperone expression and apoptotic cells. ER chaperones also showed higher expression in atherectomy specimens from patients with unstable angina pectoris than from those with stable angina. We also investigated possible signaling pathways for ER-initiated apoptosis and found that the C/EBP homologous protein (a transcription factor induced by ER stress)–dependent pathway was activated in unstable plaques. In addition, knockdown of C/EBP homologous protein expression by small interfering RNA decreased ER stress-dependent death of cultured coronary artery smooth muscle cells and THP-1 cells. Increased ER stress occurs in unstable plaques. Our findings suggest that ER stress-induced apoptosis may contribute to plaque vulnerability.

Research article

A cardiac myosin light chain kinase regulates sarcomere assembly in the vertebrate heart

Osamu Seguchi,[1] Seiji Takashima,[2,3] Satoru Yamazaki,[1] Masanori Asakura,[1] Yoshihiro Asano,[2] Yasunori Shintani,[2] Masakatsu Wakeno,[1] Tetsuo Minamino,[2] Hiroya Kondo,[2] Hidehiko Furukawa,[4] Kenji Nakamaru,[4] Asuka Naito,[4] Tomoko Takahashi,[4] Toshiaki Ohtsuka,[4] Koichi Kawakami,[5] Tadashi Isomura,[6] Soichiro Kitamura,[1] Hitonobu Tomoike,[1] Naoki Mochizuki,[1] and Masafumi Kitakaze[1]

[1]Department of Cardiovascular Medicine, National Cardiovascular Center, Suita, Osaka, Japan. [2]Department of Cardiovascular Medicine and [3]Health Care Center, Osaka University Graduate School of Medicine, Suita, Osaka, Japan. [4]Core Technology Research Laboratories, Sankyo Co. Ltd., Shinagawa, Tokyo, Japan. [5]Division of Molecular and Developmental Biology, National Institute of Genetics, Mishima, Shizuoka, Japan. [6]Hayama Heart Center, Hayama, Kanagawa, Japan.

Marked sarcomere disorganization is a well-documented characteristic of cardiomyocytes in the failing human myocardium. Myosin regulatory light chain 2, ventricular/cardiac muscle isoform (MLC2v), which is involved in the development of human cardiomyopathy, is an important structural protein that affects physiologic cardiac sarcomere formation and heart development. Integrated cDNA expression analysis of failing human myocardia uncovered a novel protein kinase, cardiac-specific myosin light chain kinase (cardiac-MLCK), which acts on MLC2v. Expression levels of cardiac-MLCK were well correlated with the pulmonary arterial pressure of patients with heart failure. In cultured cardiomyocytes, knockdown of cardiac-MLCK by specific siRNAs decreased MLC2v phosphorylation and impaired epinephrine-induced activation of sarcomere reassembly. To further clarify the physiologic roles of cardiac-MLCK in vivo, we cloned the zebrafish ortholog z-cardiac-MLCK. Knockdown of z-cardiac-MLCK expression using morpholino antisense oligonucleotides resulted in dilated cardiac ventricles and immature sarcomere structures. These results suggest a significant role for cardiac-MLCK in cardiogenesis.

Introduction

Despite recent advances in pharmacologic and surgical therapies, chronic heart failure (CHF) is still a leading cause of death worldwide (1). Currently, heart transplant is thought to be the most effective therapy for end-stage CHF. However, this approach obviously cannot be used for all of the numerous affected patients and is not suitable for patients with a mild disease state. Therefore, there is increasing demand for new therapeutic targets for CHF.

Cardiomyocytes, the most basic cellular unit of the myocardium, express several sarcomeric proteins, including myosin and actin; abnormalities in these sarcomeric proteins are major causes of idiopathic cardiomyopathies and lead to CHF (2–4). Type II myosin is the major constituent of sarcomeres. In the neck region of this protein, there are binding sites for a pair of myosin light chains, which are called the essential light chain and the regulatory light chain. Among the several paralogs of the myosin regulatory light chain in vertebrates (5), myosin regulatory light chain 2, ventricular/cardiac muscle isoform (MLC2v) is expressed in the myocardium, where it performs specific roles in cardiogenesis by contributing to the formation of sarcomeres and in increasing the Ca^{2+} sensitivity of muscle tension at submaximal Ca^{2+} concentrations (6, 7). Currently, 2 members of the myosin light chain kinase (MLCK) protein family that act on myosin regulatory light chain in muscle cells have been identified, skeletal muscle MLCK (skMLCK) and smooth muscle MLCK (smMLCK) (8). Among these MLCK family members, smMLCK, including nonmuscle isoforms, is distributed ubiquitously in various tissues and contributes to the contraction of smooth muscle and several cell activities. Conversely, skMLCK is thought to localize and function in both cardiac muscle and skeletal muscle (9); to our knowledge, no cardiac-specific MLCK has been reported to date. skMLCK-deficient mice, however, did not show any heart weight, body weight, or heart weight/body weight ratio phenotypes, despite effective knockdown of skMLCK expression (10). Additionally, there were no significant differences between the knockout and wild-type animals in regard to MLC2v phosphorylation, suggesting the existence of as-yet unknown kinases in cardiac muscle cells.

Genome-wide analyses, which have recently become available in a wide range of clinical settings, such as cancer research, allow for a global view of gene expression in certain disease states and the identification of unknown molecules and molecular pathways that can be exploited as novel therapeutic targets. CHF is a candidate disease for this type of genome-wide analysis, because of its heterogeneous properties and previous difficulties identifying responsible genes using other conventional modalities.

In this study, we performed microarray analysis of the failing human myocardium and examined the correlation between the obtained genomic data and the clinical, physiological, and biochemical characteristics of CHF. In this manner, we sought to identify candidate genes that are involved in the pathophysiology of CHF. Consequently, we identified what we believe to be a novel

Nonstandard abbreviations used: ANP, atrial natriuretic peptide; BNP, brain natriuretic peptide; CHF, chronic heart failure; cardiac-MLCK, cardiac-specific MLCK; Dd, end-diastolic dimension; Ds, end-systolic dimension; FS, fractional shortening; hpf, hours postfertilization; MI, myocardial infarction; MLC2v, myosin regulatory light chain 2, ventricular/cardiac muscle isoform; MLCK, myosin light chain kinase; M-mode, motion mode; MO, morpholino antisense oligonucleotide; p-s15MLC, antibodies for phosphorylated MLC2v; PAP, pulmonary arterial pressure; RcMK, antibodies specific for rodent cardiac-MLCK; si-cMK, siRNA targeting cardiac-MLCK; si-smMK, siRNA targeting rat smMLCK; skMLCK, skeletal muscle MLCK; smMLCK, smooth muscle MLCK; tMLC, antibodies for total MLC2v; z-, zebrafish; z-cMKaugMO, MO targeting the AUG translational start site of z-cardiac-MLCK.

Conflict of interest: The authors have declared that no conflict of interest exists.

Citation for this article: *J. Clin. Invest.* 117:2812–2824 (2007). doi:10.1172/JCI30804.

Table 1
Clinical characteristics of the patients used for microarray analysis

Pt	Age (yr)	Sex	Diagnosis	Operation	Dd (mm)	EF (%)	PAP (mmHg)	ANP (pg/ml)	BNP (pg/ml)
1	53	M	DCM, MI	Batista	88	25	20	25	90.4
2	45	M	DCM	Batista	81	39	45	85	217
3	72	M	DCM	Batista	71	14	25	86	201
4	58	M	MI	Dor	76	–	–	–	–
5	57	M	HCM, MI	Dor	52	44	41	20	80.3
6	69	M	DCM	Batista	86	19	59	100	465
7	40	M	AR	Unknown	76	42	16	52	271
8	75	M	MI	Dor	51	55	–	39	174
9	32	M	DCM	Batista	81	26	26	300	869
10	51	F	Sarcoidosis	Dor	68	35	–	89	339
11	54	M	MI	Dor	63	37	–	84	302
12	58	M	Myocarditis	Dor	77	22	–	800	2,710
N-1	27	M	Normal	–	–	–	–	–	–
N-2	24	M	Normal	–	–	–	–	–	–

AR, aortic regurgitation; DCM, dilated cardiomyopathy; EF, ejection fraction; F, female; HCM, hypertrophic cardiomyopathy; M, male; Pt, patient.

cardiac-specific MLCK (cardiac-MLCK; encoded by *MYLK3*). Phosphorylation of MLC2v by cardiac-MLCK regulated the reassembly of sarcomere structures in cultured neonatal rat cardiomyocytes. Suppression of cardiac-MLCK expression in zebrafish embryos using specific morpholino antisense oligonucleotides (MOs) led to dilation of the cardiac ventricle with incomplete sarcomere formation, suggesting critical roles for cardiac-MLCK in the heart.

Results

Identification of cardiac-MLCK from failing human myocardia using microarray analysis. To identify candidate genes involved in the pathophysiology of CHF, we used an HG-U95 Affymetrix GeneChip to analyze the gene expression profiles of failing myocardial tissues obtained from 12 patients who had undergone cardiac exclusion surgery, such as the Dor or Batista procedures, for end-stage CHF (Table 1). Figure 1A is an overview flowchart for the selection of candidate genes. Compared with those of 2 normal control samples, the expression of 626 probe sets was significantly upregulated in the failing myocardia. Of these, we selected probe sets whose expression levels were positively correlated ($r > 0.7$) with pulmonary arterial pressure (PAP) measurements (129 probe sets) and brain natriuretic peptide (BNP) mRNA levels (194 probe sets). The tissue localization of each selected probe set was then analyzed using the commercially available BioExpress database (Gene Logic Inc.). We selected 10 probe sets, for which the cardiac expression level was at least 10-fold the mean expression level of 24 other tissues, for further analysis. These probe sets represented a set of genes that included atrial natriuretic peptide (ANP), BNP, small muscle protein, and α-actin, all of which are known to be involved in heart failure, cardiac muscle remodeling, and striated muscle function. We calculated the ratios of expression in cardiac muscle to that in skeletal muscle in these probe sets. ANP (36663_at and 73106_s_at), BNP (39215_at), Importin9 (84730_at), and 75678_at exhibited expression levels that were at least 10-fold greater in the heart than in skeletal muscle. Expression levels of 75678_at, for which annotation was not available, were similar to those of ANP and BNP. We hypothesized that this unknown transcript was involved in the pathophysiology of heart failure.

Using 5′-RACE, we identified specific sequences identical to those of NM_182493 (*MYLK3*) located 4 kb upstream of the probe set sequence. The relative expression level of this candidate gene was significantly correlated with the relative PAP value (Figure 1B); in addition, the expression of this gene was restricted to the heart (Figure 1C). A homology search using the transcript sequence, particularly the sequence coding for the C-terminal kinase domain, identified *MYLK3* as a member of the MLCK family. Thus, we named the protein encoded by *MYLK3* "cardiac-MLCK." Two distinct MLCK family genes have been previously reported: *MYLK*, which encodes smMLCK, and *MYLK2*, which encodes skMLCK (8). Domain structure analysis revealed a well-conserved serine/threonine kinase domain that includes an ATP-binding site and an active serine/threonine kinase domain positioned near the C terminus of the cardiac-MLCK protein (Figure 1D). The expression patterns of the MLCK family members were confirmed by Northern blot analysis. As previously described (11), 2 major transcripts of *MYLK* were almost ubiquitously expressed. The larger transcript codes for a nonmuscle isoform of smMLCK generated by alternative splicing. Restricted expression patterns were observed for both *MYLK2* and *MYLK3*. *MYLK2* expression was only detected in skeletal muscle, whereas *MYLK3* expression was only observed in the heart (Figure 1E). *MYLK* was also found to be expressed in the heart, although its expression was not upregulated in failing myocardia as much as the expression of *MYLK3* (data not shown). To assess the physiological significance of cardiac-MLCK, we generated an adenovirus vector encoding cardiac-MLCK. In serum-free conditions, cultured neonatal rat cardiomyocytes showed predominantly disorganized sarcomere structures. Overexpression of cardiac-MLCK in cultured neonatal rat cardiomyocytes augmented sarcomere organization under serum-starved conditions (cells with organized sarcomeres, 28.7% ± 11.1% versus 3.1% ± 2.4%; $P < 0.001$; Figure 1, F and G), suggesting that cardiac-MLCK participates in sarcomere formation in cardiomyocytes.

Cardiac-specific myosin regulatory light chain is a specific substrate of cardiac-MLCK. Because this protein kinase contained a consensus kinase catalytic domain, we attempted to identify potential substrates of cardiac-MLCK. To identify physiological substrates of cardiac-MLCK, we screened murine heart homogenates using an in vitro kinase reaction. After fractionation of murine heart homogenates using a cation exchange column, aliquots of each fraction were subjected to an in vitro kinase reaction with recombinant cardiac-MLCK. Fractions 10 and 11 each contained a distinct 20-kDa band that was labeled with ^{32}P only in the presence of recombinant cardiac-MLCK (Figure 2A). This ^{32}P-labeled 20-kDa protein was purified (Figure 2B) and analyzed using matrix-assisted laser desorption/ionization-time-of-flight mass spectrometry and peptide mass fingerprinting. The 20-kDa protein contained fragments with amino acid sequences that were homologous to murine MLC2v (Figure 2C). No additional ^{32}P-labeled proteins were detected in fractions obtained following cation or anion exchange column purification. Further analysis of this phosphorylation event in vitro revealed endogenous MLC2v, purified from murine heart homogenates, was phosphorylated by recombinant cardiac-MLCK in a Ca^{2+}-calmodulin–dependent manner (Figure 2D). Thus, we conclude that cardiac-MLCK is a calmodulin-dependent kinase.

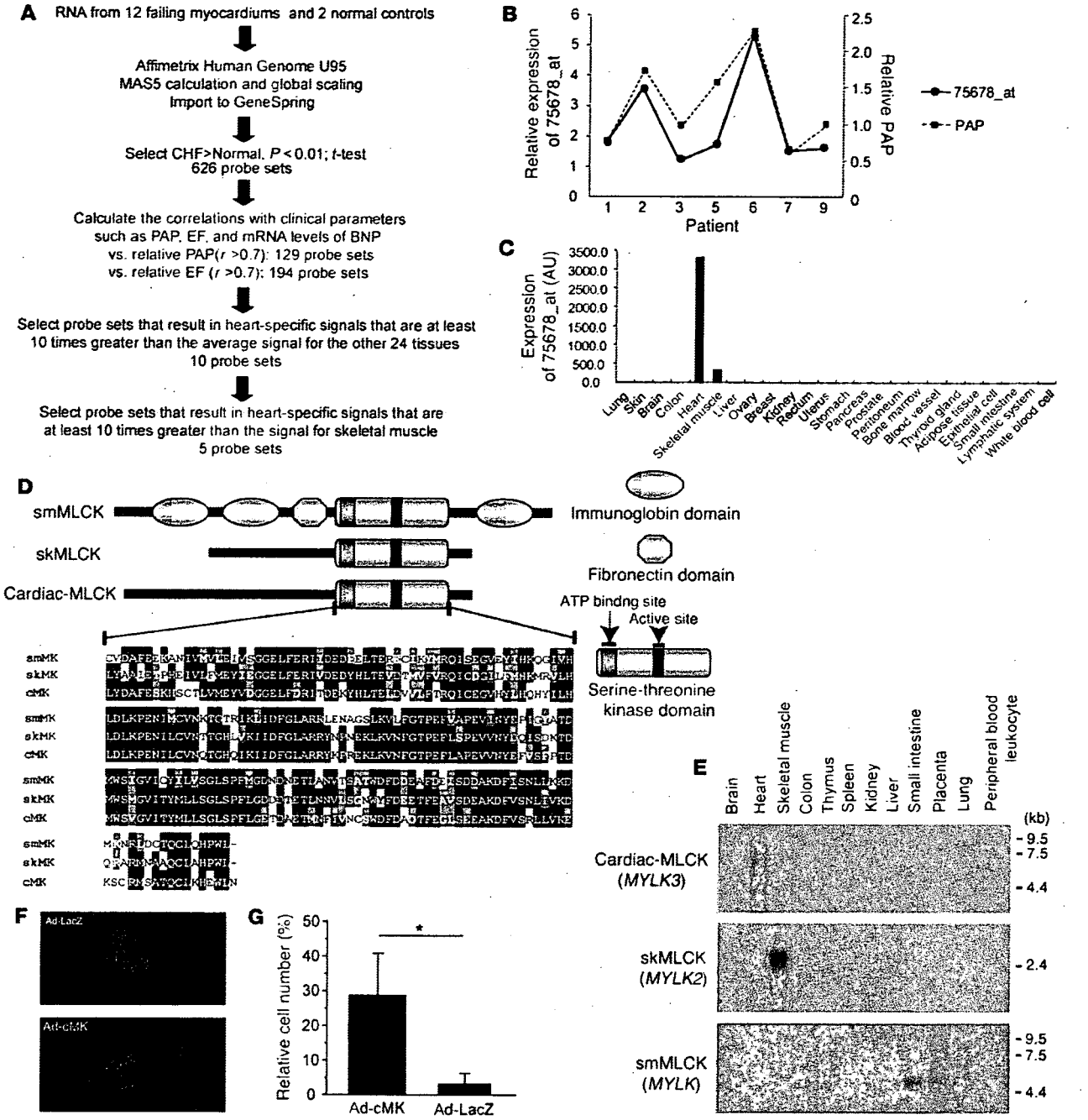

Figure 1

Microarray analysis for candidate gene selection. (**A**) Flowchart for the selection of candidate genes. (**B**) The relative expression levels of 75678_at correlated well with the relative PAP values in the respective patients. (**C**) Tissue localization of the candidate gene expression was analyzed using the GeneExpress database; 75678_at was specifically expressed in the heart. (**D**) Each MLCK family member possesses a highly conserved serine-threonine kinase domain in the C-terminal region of the protein. Amino acid residues on black backgrounds are the most commonly conserved residues at each position; residues on gray backgrounds are similar to the consensus amino acids. (**E**) Expression analysis of MLCK family members using multiple human tissue Northern blot membranes. The 2 transcripts transcribed from *MYLK* (encoding smMLCK) were ubiquitously expressed with the exception of skeletal muscle, thymus, and peripheral blood leukocytes. In contrast, *MYLK2* (encoding skMLCK) and *MYLK3* (encoding cardiac-MLCK) were only expressed in skeletal muscle and heart, respectively. (**F**) Fluorescence microscopy of cardiomyocytes cultured in serum-free conditions and infected with adenovirus encoding LacZ (Ad-LacZ) revealed predominantly round-shaped cells with disorganized sarcomere structures. Infection with adenovirus encoding cardiac-MLCK (Ad-cMK) at a MOI of 120 increased the number of the cells with organized sarcomere structures. Original magnification, ×1,000. (**G**) The percentage of cells with organized sarcomeres was significantly higher in cardiomyocytes infected with adenovirus encoding cardiac-MLCK than in those infected with adenovirus encoding LacZ. Values are mean ± SEM. $^*P < 0.001$.

Next, we generated polyclonal antibodies specific for rodent cardiac-MLCK (RcMK). Antibodies that detected phosphorylated MLC2v (p-s15MLC; anti-rodent serine 15 phosphorylated MLC2v) and total MLC2v (tMLC) were also generated. RcMK detected rat cardiac-MLCK from whole-cell cardiomyocyte extracts as well as recombinant FLAG-tagged murine cardiac-MLCK (Figure 2E). Phosphorylated MLC2v and nonphosphorylated MLC2v could be clearly separated using urea-glycerol gel electrophoresis (12). tMLC detected both phosphorylated and nonphosphorylated MLC2v, whereas p-s15MLC specifically detected the phosphorylated form of MLC2v (Figure 2F). Overexpression of cardiac-MLCK increased the levels of phosphorylated MLC2v in cultured cardiomyocytes (Figure 2G). However, there was no effect on the expression of other sarcomere proteins involved in sarcomere organization such as troponin T, desmin, and α-actinin. mRNA expression of ANP and β myosin heavy chain, representative markers of cardiac hypertrophy, were also unaffected by cardiac-MLCK overexpression (data not shown). To further investigate the phosphorylation of MLC2v by endogenous cardiac-MLCK, we used specific siRNAs targeting cardiac-MLCK (si-cMKs). These siRNAs effectively suppressed the level of cardiac-MLCK mRNA by more than 70%, as determined using quantitative real-time PCR 24 hours after transfection (Figure 2H). These siRNAs also effectively suppressed the level of cardiac-MLCK protein and the amount of phosphorylated MLC2v 60–72 hours after transfection (Figure 2I), whereas no remarkable effects were seen for the expression of other sarcomere proteins. On the contrary, suppression of smMLCK expression, which is also distributed in heart, using siRNA targeting rat smMLCK (si-smMK) did not change either the phosphorylation status of MLC2v or the expression of sarcomere proteins (Figure 2J). These results indicated that cardiac-MLCK predominantly phosphorylates MLC2v, which is selectively expressed in cardiomyocytes. Thus, cardiac-MLCK may regulate morphologic change in cardiomyocytes, including sarcomere organization, through MLC2v phosphorylation.

Cardiac-MLCK regulates sarcomere assembly in cultured cardiomyocytes. To elucidate the precise role of cardiac-MLCK in the sarcomere structure, we analyzed the effects of MLC2v phosphorylation on sarcomeres in cultured neonatal rat cardiomyocytes. Polymerized actin stained with rhodamine-phalloidin revealed a regularly organized pattern of striations (Figure 3A). Phosphorylated MLC2v labeling with p-s15MLC demonstrated a similar striated pattern, although the labeling was predominantly observed in the A-band region, a portion of the sarcomere primarily made up of thick filaments (Figure 3, B–D). Diffuse cytosolic fluorescent labeling was seen when cardiac-MLCK was labeled with RcMK (Figure 3, E–G).

When cardiomyocytes were cultured in serum-free conditions, the organized striation pattern of actin was disrupted and the phosphorylated MLC2v-specific signal decreased (Figure 3K). To evaluate the morphologic changes observed in cardiomyocytes upon activation of endogenous cardiac-MLCK, we treated cardiomyocytes cultured under serum-free conditions with epinephrine. Stimulation of G protein–coupled receptors with epinephrine should activate cardiac-MLCK by increasing intracellular Ca^{2+} concentrations (13). A marked upregulation of MLC2v phosphorylation was obtained following treatment with 2 μM epinephrine (Figure 3H). Epinephrine-induced phosphorylation of MLC2v, which was observed as early as 5 minutes after stimulation, peaked within 30 minutes (Figure 3I). Treatment of the cardiomyocytes cultured in serum-free conditions with 2 μM epinephrine also induced reassembly of sarcomere structures and MLC2v phosphorylation (Figure 3, J, K, and L). To confirm the relevance of MLC2v phosphorylation by cardiac-MLCK, we introduced si-cMKs into cardiomyocytes and analyzed the sarcomere patterns in these cells. The level of phosphorylated MLC2v was reduced 72 hours after transfection with the si-cMKs; however, we did not observe any remarkable changes in the structures of the sarcomeres in cardiomyocytes cultured with serum. The sarcomeres of control siRNA– and si-cMK–treated cells contained organized filament structures (cells with organized sarcomeres, 97.0% ± 1.0% versus 90.0% ± 1.0%; NS; Figure 4, A–F and I). In contrast, the knockdown of cardiac-MLCK produced significant effects on sarcomere reassembly. si-cMK inhibited sarcomere reassembly after epinephrine treatment in cardiomyocytes cultured under serum-free conditions (cells with organized sarcomeres, 76.0% ± 8.5% versus 43.6% ± 7.0%; $P < 0.005$; Figure 4, A–F and I). We also confirmed the phosphorylation of MLC2v using immunoblot analysis (Figure 4G). The results of the immunoblot analysis are quantified in Figure 4H, and the relative MLC2v phosphorylation levels in this experiment exhibited a similar pattern as the percentages of cardiomyocytes with organized sarcomeres (Figure 4I), except in baseline, serum-containing conditions. These data suggest that MLC2v phosphorylation by cardiac-MLCK plays a critical role in initiating sarcomere reassembly.

Cardiac-MLCK is essential for normal cardiac development and function in zebrafish embryos. In order to further evaluate the physiologic roles of cardiac-MLCK, genetically engineered animals must be examined. In mice, however, targeted deletion of the cardiac ventricular myosin light chain, a specific substrate of cardiac-MLCK, was embryonic lethal at embryonic day 12.5 (6). Because cardiac-MLCK is an upstream modulator of MLC2v, deletion of the gene encoding cardiac-MLCK could also be embryonic lethal. Therefore, we performed in vivo knockdown experiments in *Danio rerio*, in which the phenotype generated by disrupting the functions of a targeted gene can be analyzed even if loss of the gene's functions is fatal. First, we generated a zebrafish cDNA library from which we cloned the zebrafish ortholog of *MYLK3* (*zmylk3*; encoding z-cardiac-MLCK). The amino acid sequence of cardiac-MLCK is highly similar to those of other vertebrate orthologs, especially within the C-terminal serine/threonine kinase domain (Figure 5A). Furthermore, like *MYLK3*, *zmylk3* is located between the genes VPS35 and NP001001436.1 (Assembly Zv5sc; Wellcome Trust Sanger Institute), indicating that this was the region of synteny between human and zebrafish. We also performed whole-mount in situ hybridizations using *zmylk3*-specific probes; the results indicated that *zmylk3* was expressed only in the heart at 24 and 48 hours postfertilization (hpf; Figure 5, B–I).

We injected zebrafish embryos with a specific MO directed against the AUG translational start site of the z-cardiac-MLCK mRNA (z-cMKaugMO). At 33 hpf, compared to control mock-injected zebrafish embryos, the heart region was slightly swollen in the z-cMKaugMO morphants. At 48 hpf, ventral swelling was observed in 45.6% ± 6.8% of the z-cMKaugMO morphants (Figure 6A). The ventral swelling became more apparent at 72 hpf (Figure 6B). In contrast, zebrafish embryos injected with an MO containing 5-base mismatches compared with z-cMKaugMO were indistinguishable from control zebrafish embryos (Figure 6C). We further examined the effects of 3 additional MOs, which were targeted to delete specific exons of z-cardiac-MLCK and z-MLC2v. Of these MOs, 2 were directed against the splice donor and acceptor

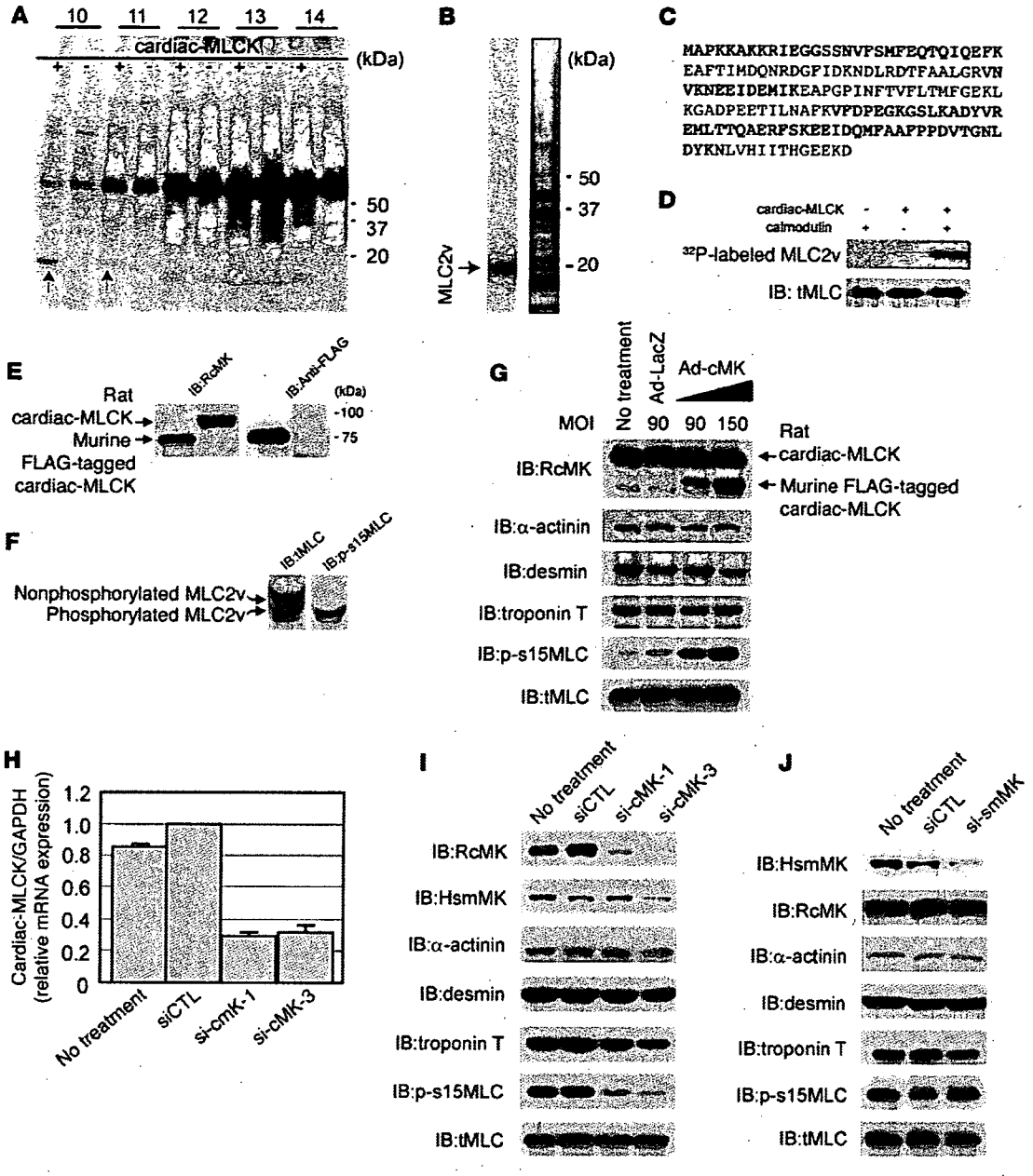

Figure 2

Identification of MLC2v as a specific substrate of cardiac-MLCK. (**A**) A putative 20-kDa substrate that was labeled with P^{32} in the presence of cardiac-MLCK was identified in fractionated murine myocardium extracts (arrows). Fraction numbers are shown at top. (**B**) P^{32}-labeled MLC2v was purified and visualized by autoradiography (left lane) and silver staining (right lane). (**C**) Peptides from the purified protein, which matched the sequences of murine MLC2v, are shown in red. (**D**) Purified MLC2v from murine myocardia was phosphorylated by cardiac-MLCK in a Ca^{2+}-calmodulin–dependent manner. (**E**) RcMK detected rat cardiac-MLCK from cultured cardiomyocyte cell extracts and FLAG-tagged murine cardiac-MLCK. (**F**) Nonphosphorylated MLC2v and phosphorylated MLC2v were separated using urea-glycerol gel electrophoresis. tMLC and p-s15MLC were confirmed to specifically detect each target protein. (**G**) Overexpression of murine cardiac-MLCK in cultured cardiomyocytes following infection with an adenovirus vector encoding murine cardiac-MLCK at MOIs of 90 and 150 upregulated the phosphorylation of MLC2v in a dose-dependent manner. Endogenous rat cardiac-MLCK is shown at top; overexpressed murine cardiac-MLCK is shown below. (**H** and **I**) Both si-cMK-1 and si-cMK-3 effectively suppressed the mRNA (**H**) and protein levels (**I**) of cardiac-MLCK, resulting in reduced phosphorylation of MLC2v. smMLCK, α-actinin, desmin, and troponin T were not affected by suppression of cardiac-MLCK expression. siCTL, control siRNA. (**J**) The protein levels of smMLCK were effectively decreased by si-smMK; no remarkable changes were observed in protein levels of phosphorylated MLC2v or other sarcomere-related proteins.

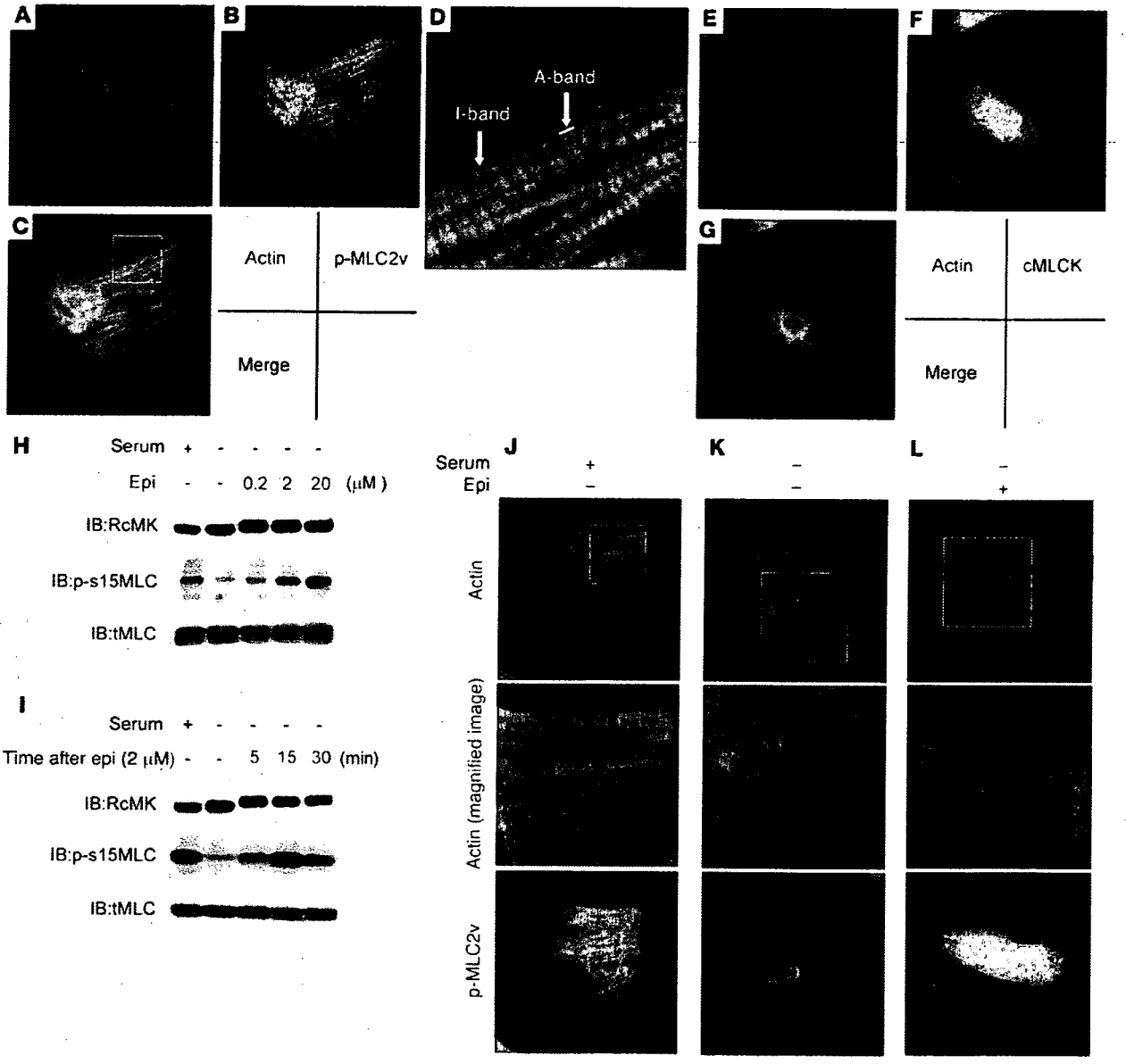

Figure 3

Epinephrine treatment induced sarcomere assembly through MLC2v phosphorylation. Original magnification, ×1,000 (**A–C** and **E–G**). (**A–D**) Polymerized actin stained with rhodamine-phalloidin (**A**) as well as phosphorylated MLC2v labeled with p-s15MLC (**B**) exhibited regular patterns of striation. (**C**) Merged image of **A** and **B**. (**D**) Higher magnification of boxed area in **C** revealed that rhodamine-phalloidin predominantly stained the I-band, whereas phosphorylated MLC2v (p-MLC2v) was localized in the A-band. Original magnification, ×4,000 (**D**). (**E–G**) Cardiac-MLCK (cMLCK) labeled with RcMK showed a diffuse cytosolic labeling pattern. (**H**) Cultured cardiomyocytes were stimulated with 0.2–20 μM epinephrine (Epi), which upregulated MLC2v phosphorylation in a dose-dependent manner. (**I**) Cultured cardiomyocytes were stimulated with 2 μM epinephrine for the indicated time periods. Epinephrine-induced phosphorylation of MLC2v in cultured cardiomyocytes was observed as early as 5 minutes after stimulation; maximal phosphorylation was obtained after approximately 30 minutes. (**J–L**) Cardiomyocytes cultured with serum contained organized patterns of striation and a moderate level of MLC2v phosphorylation. Middle panels show higher magnification of boxed regions in top panels. Cardiomyocytes cultured in serum-free conditions were incubated in the absence (**K**) or presence (**L**) of 2 μM epinephrine. (**K**) Cardiomyocytes cultured under serum-free conditions contained disorganized, punctuated actin staining with a reduced level of MLC2v phosphorylation. (**L**) Stimulation with epinephrine provoked rapid sarcomere reassembly and augmented MLC2v phosphorylation. Original magnification, ×1,000 (**J–L**, upper and lower panels); ×3,000 (**J–L**, middle panels).

sites of exons 4 and 6 of z-cardiac-MLCK, respectively. Deletion of exon 4 caused a frameshift and resulted in premature termination of the transcript. Exon 6 includes the catalytic center of z-cardiac-MLCK, and its deletion was expected to diminish the protein's kinase activity. The third MO was designed to delete exon 2 of z-MLC2v, which includes the phosphorylatable serine. These 3